Phenotypic and functional characterization of corneal endothelial cells during in vitro expansion

Ricardo F. Frausto[1], Vinay S. Swamy[1], Gary S. L. Peh[2], Payton M. Boere[1], E. Maryam Hanser[1], Doug. D. Chung[1], Marco Morselli[3,4], Liyo Kao[5], Rustam Azimov[5], Matteo Pellegrini[3,4,6,7], Ira Kurtz[5,8], Jodhbir S. Mehta[2] and Anthony J. Aldave[1]

[1]Stein Eye Institute, David Geffen School of Medicine at UCLA, Los Angeles, California, USA; [2]Tissue Engineering and Stem Cell Group, Singapore Eye Research Institute, Singapore; [3]Department of Molecular, Cell and Developmental Biology, UCLA, Los Angeles, California 90095, USA; [4]Institute for Quantitative and Computational Biology, UCLA, Los Angeles, California 90095, USA; [5]Division of Nephrology, David Geffen School of Medicine at UCLA, Los Angeles, California 90095; [6]Molecular Biology Institute, UCLA, Los Angeles, California 90095, USA; [7]Jonsson Comprehensive Cancer Center, UCLA, Los Angeles, California 90095, USA; [7]Brain Research Institute, UCLA, Los Angeles, California 90095

Support provided by National Eye Institute Grants R01 EY022082 (A.J.A.), P30 EY000331 (core grant), the Walton Li Chair in Cornea and Uveitis (A.J.A.), Eye Bank Association of America Richard Lindstrom Research Grant (AJA), the Stotter Revocable Trust (SEI Cornea Division), an unrestricted grant from Research to Prevent Blindness (A.J.A.), National Institute of Diabetes and Digestive and Kidney Diseases 1R01 DK077162 (I.K.), the Allan Smidt Charitable Fund (I.K.), Ralph Block Family Foundation (I.K.), and U.S. Department of Energy Office of Science, Office of Biological and Environmental Research Program DE-FC02-02ER63421 (M.M).

Correspondence:

Anthony J. Aldave, M.D.

Professor of Ophthalmology

Stein Eye Institute, 200 Stein Plaza, UCLA, Los Angeles, CA 90095-7003

Tele: 310.206.7202 Fax: 310.794.7906 Email: aldave@jsei.ucla.edu

SUMMARY

The advent of cell culture-based methods for the establishment and expansion of human corneal endothelial cells (CEnC) has provided an available source of transplantable corneal endothelium, with a significant potential to challenge the one donor-one recipient paradigm. However, concerns over cell state identity remain, and a comprehensive characterization of the cultured CEnC has not been performed. To this end, we compared two established CEnC culture methods by assessing cell function and characterizing the transcriptomic changes that occur during in vitro expansion. In confluent monolayers, low mitogenic culture conditions preserved corneal endothelial cell state identity better than culture in high mitogenic conditions. Expansion by continuous passaging induced replicative cell senescence. Transcriptomic analysis of the senescent phenotype identified a cell senescence signature distinct for CEnC. We identified activation of both classic and new cell signaling pathways that may be targeted to prevent senescence, a significant barrier to realizing the potential clinical utility of in vitro expansion.

Keywords: CEnC, cornea, endothelium, endothelial cells, senescence, transcriptomics, transplantation, cell barrier, cell migration, pump function

INTRODUCTION

The worldwide shortage of donor corneal tissue for the treatment of corneal endothelial dysfunction necessitates the development of viable alternatives to the paradigm of one donor cornea being used for only one recipient (Mehta et al., 2019; Okumura et al., 2014b; Soh et al., 2017). Corneal endothelial cell (CEnC) dysfunction is the primary indication for corneal transplantation both in the United States and worldwide, and while endothelial keratoplasty represents a significant advance in the surgical management of corneal endothelial dysfunction, the worldwide shortage of surgical-grade donor corneas and the lack of adequately trained surgeons in the majority of countries, as well as a variety of associated intraoperative and postoperative complications, have significantly limited the impact of endothelial keratoplasty on visual impairment worldwide due to corneal endothelial dysfunction (Deng et al., 2015; Lass et al., 2017; Van den Bogerd et al., 2018). The in vitro generation of stem cell-derived corneal endothelial-like cells (Yamashita et al., 2018), immortalized CEnC lines (Schmedt et al., 2012; Valtink et al., 2008) and expansion of primary CEnC from cadaveric donor corneal tissue (Okumura et al., 2014b; Parekh et al., 2016; Peh et al., 2019) have challenged the one donor-one recipient paradigm of corneal transplantation. Nevertheless, in vitro culture poses its own challenges, including unwanted changes in cell phenotype (e.g., endothelial to fibroblastic) and progression towards replicative senescence that limits cell numbers (Sheerin et al., 2012; Soh et al., 2017). In addition, the quality of the donor tissue from which the CEnC are derived is critical in the successful establishment of an in vitro CEnC culture. Donor age significantly impacts culture success rate, with the optimal age being less than 40 years old. Reduced success rates from older donors are correlated with an appearance of senescence-associated markers ex vivo (Mimura and Joyce, 2006), and this is believed to significantly limit re-entry into the cell cycle even in the presence of potent mitogenic factors. While senescence is generally an irreversible cell state (Campisi, 2013), CEnC from younger donors are characterized by a quiescent cell state (G1 cell cycle arrest), which is a reversible mitotic arrest that enables these cells to undergo mitogen-induced cell cycle re-entry (Joyce, 2005). Donor age and other factors (e.g., days in preservation medium, donor medical history, cell count) dictate the success of establishing in vitro cultures (Soh et al., 2017). This makes

identifying an optimal in vitro culture protocol essential for ensuring consistent establishment and expansion of CEnC .

The corneal endothelium is a neuroectoderm-derived tissue that is located on the posterior surface of the cornea and is a semipermeable monolayer of mitotically inactive (i.e., quiescent) CEnC. A critical functional property of the corneal endothelium is to maintain the corneal stroma in a relatively dehydrated state. This process ensures that the collagen fibers of the stroma retain an ultrastructural organization essential for corneal transparency. The pump-leak hypothesis is believed to best explain the role that the endothelium plays in maintaining a relatively dehydrated stroma. Passive movement of water from the aqueous humor to the stroma (i.e., leak) and active transport of solutes (i.e., pump) in the opposite direction are regulated by the CEnC barrier formation (i.e., tight junctions, cell adhesion) and expression of solute transporters (e.g., Na/K ATPases, SLC4A11) (Gottsch et al., 2003). Mutations in genes associated with transporter function (e.g., *SLC4A11*) or CEnC identity (e.g., *ZEB1, TCF4*) lead to stromal edema and loss of corneal clarity (Baratz et al., 2010; Krafchak et al., 2005; Vithana et al., 2006; Wieben et al., 2012). In general, loss of barrier integrity, dysfunction of solute transporters or a significant decrease in CEnC density leads to loss of corneal clarity that necessitates corneal transplantation. Endothelial cell failure constitutes the primary indication for corneal transplantation in the U.S., serving at the indication for 55% of all keratoplasty procedures performed in 2018 (2018). While endothelial keratoplasty remains the primary method for managing endothelial cell dysfunction in the U.S., the aforementioned factors that have limited the impact of endothelial keratoplasty on decreasing the global burden of vision loss from endothelial dysfunction necessitates the development of alternative therapeutic interventions.

To achieve this goal, we assessed two previously reported methods for establishing cultures of primary CEnC (Bednarz et al., 1998; Peh et al., 2015) by using a multipronged approach. We determined the impact of in vitro expansion on CEnC gene expression by performing a transcriptomics analysis, and identified gene expression features of replicative senescence. In addition, we performed a variety of assays to determine the impact of these two methods on essential CEnC functions. We identified new

potential targets for suppressing cellular senescence, and confirmed that a relatively low mitogenic environment is better at maintaining the CEnC phenotype in vitro (Peh et al., 2015). These findings form the basis for continued development of in vitro culture and expansion of primary CEnC for their eventual use in cell replacement therapy for the management of corneal endothelial loss or dysfunction.

98 **METHODS**

99 **Primary corneal endothelial cell cultures**

100 Corneas used in this study were obtained from commercial eye banks (Table S1). Criteria used for
101 selection of high quality donor corneal tissue were: 1) donor younger than 40 years (mean: 17.6; range: 2-
102 35); 2) no donor history of diabetes or corneal disease; 3) endothelial cell density greater than 2300
103 cells/mm^2 (mean: 3019; range: 2387-3436); 4) death to preservation less than 12 hours, if body not
104 cooled, or less than 24 hours, if body cooled; and 4) death to culture less than 15 days (mean: 6; range: 2-
105 14). Descemet membrane with attached endothelium was stripped from the stroma using the method
106 commonly employed in preparation of the donor cornea for Descemet membrane endothelial keratoplasty.
107 Seven independent CEnC cultures were established using two previously described protocols with minor
108 modifications (Bednarz et al., 1998; Peh et al., 2015). One method utilizes trypsin for dissociation of
109 endothelial cells from Descemet membrane, followed by seeding on laminin coated cell culture plastic,
110 and culturing in a 1:1 mixture of F12-Ham's and M199 (F99) medium. The second method utilizes
111 collagenase A for dissociation of endothelial cells from Descemet membrane. This is followed by seeding
112 on collagen IV coated cell culture plastic, and culturing initially in Endothelial SFM (M5) followed by
113 culturing in a 1:1 mixture of F12-Ham's and M199 (M4) medium. When cells reach confluence, the
114 medium is changed back to M5 medium for establishment and maintenance of the CEnC phenotype. Cell
115 passaging is performed with TrypLE Select (Thermo Fisher Scientific). Cells isolated using each protocol
116 are referred to as F99 cells or M5 (M4/M5 or dual media) cells to indicate the method used to establish
117 the cultures.

118

119 **Total RNA isolation**

120 Primary CEnC were lysed in TRI Reagent (Thermo Fisher) and total RNA was prepared as per the
121 manufacturer's instructions. RNA preparations were subsequently purified using the RNeasy Clean-Up
122 Kit (Qiagen, Valencia, CA). The quality of the total RNA was assessed with both the Agilent 2100

123 Electrophoresis Bioanalyzer System (Agilent Technologies, Inc., Santa Clara, CA) and the Agilent
124 TapeStation 2200 (Agilent Technologies, Inc.).
125
126 **RNA-sequencing and data processing**
127 RNA was isolated and RNA-seq libraries were prepared using the KAPA mRNA HyperPrep Kit with an
128 automated liquid handler (Janus G3 – PerkinElmer) according to the manufacturer's instructions. Library
129 preparation was performed at the UCLA Institute for Quantitative and Computational Biology. DNA
130 libraries were submitted to the UCLA Technology Center for Genomics and Bioinformatics for
131 sequencing, which was performed on the Illumina HiSeq 3000 platform. All RNA-seq data were single-
132 end 50 base reads. Reads were aligned to the human GRCh38.p12 genome, and transcripts were
133 quantified using the kallisto (v0.44.0) program (Bray et al., 2016) with the Ensembl Annotation Release
134 version 92. Quantities were given in transcripts per million (TPM), and differential gene expression
135 analysis was performed with the Sleuth (v0.30.0) R-package (Pimentel et al., 2017). Differential
136 expression was tested using a likelihood ratio test (negative binomial test), and corrected for multiple
137 testing using the Benjamini-Hochberg correction. Given the sporadic availability of donor corneas, each
138 of the seven cultures was established as an individual batch. To account for batch effects in the data, we
139 included batch number (i.e., culture number) as a covariate in the model used to test for differential
140 expression. The following thresholds defined differential expression: fold change>1.5, TPM>11.25 and q-
141 value<0.05. Of note, our background threshold was 7.5 TPM, and the threshold of 11.25 TPM (stated
142 above) accounted for the 1.5 fold change criterion. With the goal of achieving a balance between Type I
143 and Type II errors, the background threshold was selected to retain genes with low expression (e.g., *ZEB1*
144 with a TPM of ~25 TPM), but was sufficiently robust to exclude many genes with low (<7.5 TPM)
145 abundance values. RNA-seq data generated from ex vivo corneal cell types were obtained from the GEO
146 DataSets database (accession GSE121922). RNA-seq data generated for this study were submitted to
147 GEO DataSets and assigned accession number GSE132204.
148

149 **Gene ontology and pathway analysis**

150 Gene ontology (GO) and pathway analysis on gene symbols only was performed using the web-based tool
151 gProfiler (version: e94_eg41_p11_04285a3). The three main GO categories are Molecular Function
152 (MF), Biological Process (BP) and Cellular Component (CC) (data version: release/2018-12-28).
153 Databases used for pathway analysis were Kyoto Encyclopedia of Genes and Genomes (KEGG)
154 pathways (version: KEGG FTP Release 2019-01-07), REACTOME (REAC) pathways (classes: 2019-1-
155 24), and WikiPathways (WP)(version: 20190110). The g:SCS method for computing multiple testing
156 correction was used for selecting significantly enriched GO terms and pathways identified by gProfiler.
157 Ingenuity Pathway Analysis software (Qiagen; build: 486617M) was used to determine the pathways
158 enriched and activated in our lists of differentially expressed genes.

159

160 **Quantitative PCR**

161 Quantitative polymerase chain reaction (qPCR) was performed to validate gene transcript abundances
162 observed by RNA-seq. Total RNA (100 ng) was subjected to first-strand cDNA synthesis using the
163 SuperScript III First-Strand Synthesis kit (Thermo Fisher Scientific) with oligo-dT primers. Reactions
164 were performed on the LightCycler 480 System (Roche) using the KAPA SYBR FAST qPCR Kit
165 (Roche) and gene-specific oligonucleotide primers obtained from the Harvard Primer Bank database
166 (Spandidos et al., 2008; Spandidos et al., 2010; Wang and Seed, 2003) or designed using the NCBI
167 Primer-BLAST tool (Table S2). Relative transcript abundances were calculated in comparison with the
168 housekeeping gene *RAB7* using the comparative Ct ($2^{-\Delta Ct}$) method (Livak and Schmittgen, 2001).
169 Transcript quantities were graphed as $2^{-\Delta Ct}$.

170

171 **Capillary-based, automated protein immunodetection assay**

172 Cells were lysed with RIPA buffer and whole-cell lysates were prepared and processed for protein
173 detection using the Wes separation 12-230 kDa capillary cartridges (Protein Simple). Separation and
174 detection were performed as per the manufacturer's instructions. Quantification and data analysis were

175 performed using the Compass for SW software (version 3.1.7; build ID: 1205). Primary antibodies are
176 listed in Table S3).
177
178 **Morphometric analysis**
179 At each passage, we acquired phase contrast images of confluent monolayers established in either F99 or
180 M5. Image acquisition was performed with the Leica DMIL LED inverted microscope (Leica
181 Microsystems), the N PLAN L 20x/0.35 PH1 objective, and the SPOT Insight color camera
182 (Diagnostic Instruments, Inc.). Images were captured with the SPOT software (version 4.6). Image
183 analysis was performed using ImageJ 1.51h (National Institutes of Health). We created regions of
184 interest (ROI) by outlining the periphery of at least 20 representative cells using the freehand tool.
185 ImageJ output the values for area (um2) and circularity (ratio) for the selected ROI.
186
187 **Cell barrier assay**
188 The electrode array 8W10E+ ECIS (Applied BioPhysics) was stabilized with F99 or M5 medium. The
189 array surface was coated with 40 μg/cm^2 chondroitin sulfate A (Sigma-Aldrich) and 400 ng/cm^2 laminin
190 (Sigma-Aldrich) in phosphate-buffered saline (PBS) for two hours (for F99 cells) or with 7.5 μg/cm^2
191 collagen IV (Sigma-Aldrich) in 1x HEPES for 30 min (for M5 cells). Cells were seeded at a density to
192 achieve 100% confluence shortly after seeding, and were incubated in the arrays at room temperature for
193 one hour to facilitate even distribution. After seeding and preliminary cell attachment, arrays were
194 positioned into a 16-well array station and connected to the ECIS Zθ instrument to measure electric
195 impedance (Ω at 4000 Hz) for 4 days. Cell-cell (R_b, Ω • cm^2) and cell-substrate (α, Ω$^{1/2}$ • cm) adhesion
196 were modeled from the electric impedance data obtained at 4000 Hz (Stolwijk et al., 2015).
197
198 **Transporter assays**
199 Lactate (SLC16A1), bicarbonate (SLC4A4) and proton (SLC4A11) transport were monitored by

200 measuring free H^+ concentration (pHi) with a microscope fluorometer (Kao et al., 2016) using the
201 fluorescence-based (dual-excitation 500 nm and 440 nm) ratiometric pH indicator BCECF (Thermo
202 Fisher Scientific), which was pre-loaded into the cells prior to substrate exposure.
203 *SLC16A1 transporter*: BCECF loading was performed in lactate-free solution (20mM Na gluconate,
204 120mM NaCl, 1mM $CaCl_2$, 1mM $MgCl_2$, 2.5mM K_2HPO_4, 5mM dextrose and 5mM HEPES, pH 7.4).
205 Fluorescence was monitored until a stable pH_i was achieved. Subsequently, the lactate-free buffer was
206 replaced by perfusion with lactate-containing solution (20mM Na lactate in place of 20mM Na
207 gluoconate) for about 200 seconds and then switched back to the lactate-free solution.
208 *SLC4A4 transporter*: BCEFC loading was performed in bicarbonate-free solution (140mM TMACl,
209 2.5mM K2HPO4, 1mM CaCl2, 1mM MgCl2, 5mM Dextrose and 5mM HEPES, pH 7.4). After pH_i
210 stabilization was attained, the solution was replaced by perfusion with a solution containing
211 tetramethylammonium bicarbonate (115mM TMACl and 25mM TMAHCO3 in place of 140mM TMACl
212 and 5mM HEPES). Perfusion was performed for about 200 seconds and then switched to a solution
213 containing sodium bicarbonate (115mM NaCl, 2.5mM K2HPO4, 1mM CaCl2, 1mM MgCl2, 5mM
214 Dextrose and 25mM NaHCO3, pH 7.4), and fluorescence was monitored for an additional 400-600
215 seconds.
216 *SLC4A11 transporter*: BCECF loading was performed in HEPES buffer (110mM KCl, 35mM TMACl
217 and 5mM HEPES, pH 7.4). Once pH_i stabilized, a second HEPES buffer (110 mM KCl, 35 mM TMACl
218 and 5 mM HEPES pH 6.2) was replaced by perfusion and pH_i was monitored for approximately 800
219 seconds.
220 **Cell migration assay**
221 A non-wounding method to assess cell migration was used. Two-well silicone inserts (ibidi GmbH), each
222 creating a 500um gap, were placed onto cell culture treated plastic. Wells were coated as described above
223 for F99 and M5 cells. After cell isolation was performed, cells were seeded into each well and allowed to
224 grow to confluence. Cell migration was initiated by removing the insert and was monitored for up to 60
225 hours by phase-contrast microscopy. Images were acquired using the Leica DMIL LED inverted

226 microscope (Leica Microsystems) and the N PLAN L 20x/0.35 PH1 objective. Image capture was
227 performed with the Leica DFC3000 G monochrome camera controlled with the Leica Application
228 Suite X software (version 3.0.3.16319). Gap closure was measured at 22 hours and cell size was
229 measured at 60 hours using ImageJ 1.51h software (National Institutes of Health).

RESULTS

In vitro expansion of CEnC induces senescence-associated morphogenesis

The morphogenic effects of culture in high mitogenic (F99) and low mitogenic (M5) conditions on primary CEnC were examined (Fig. 1). Phase contrast images were acquired at each passage when confluent monolayers were established (Fig. 1B and Fig. S1). Morphometric analysis was performed at each passage (Fig. 1C). Up to passage 3, the area occupied by each cell was greater in F99, compared with cells in M5, but the effect of medium on the curves was not statistically significant ($p=0.065$). Cell circularity, which measures the degree to which a cell shape resembles a circle (1.0 is a perfect circle), was greater at all passages for cells in M5 medium, compared with cells in F99. The effect of medium on the curves for circularity was statistically significant ($p=0.042$). As the value approaches 0, cell shape is increasingly irregular and/or elongated.

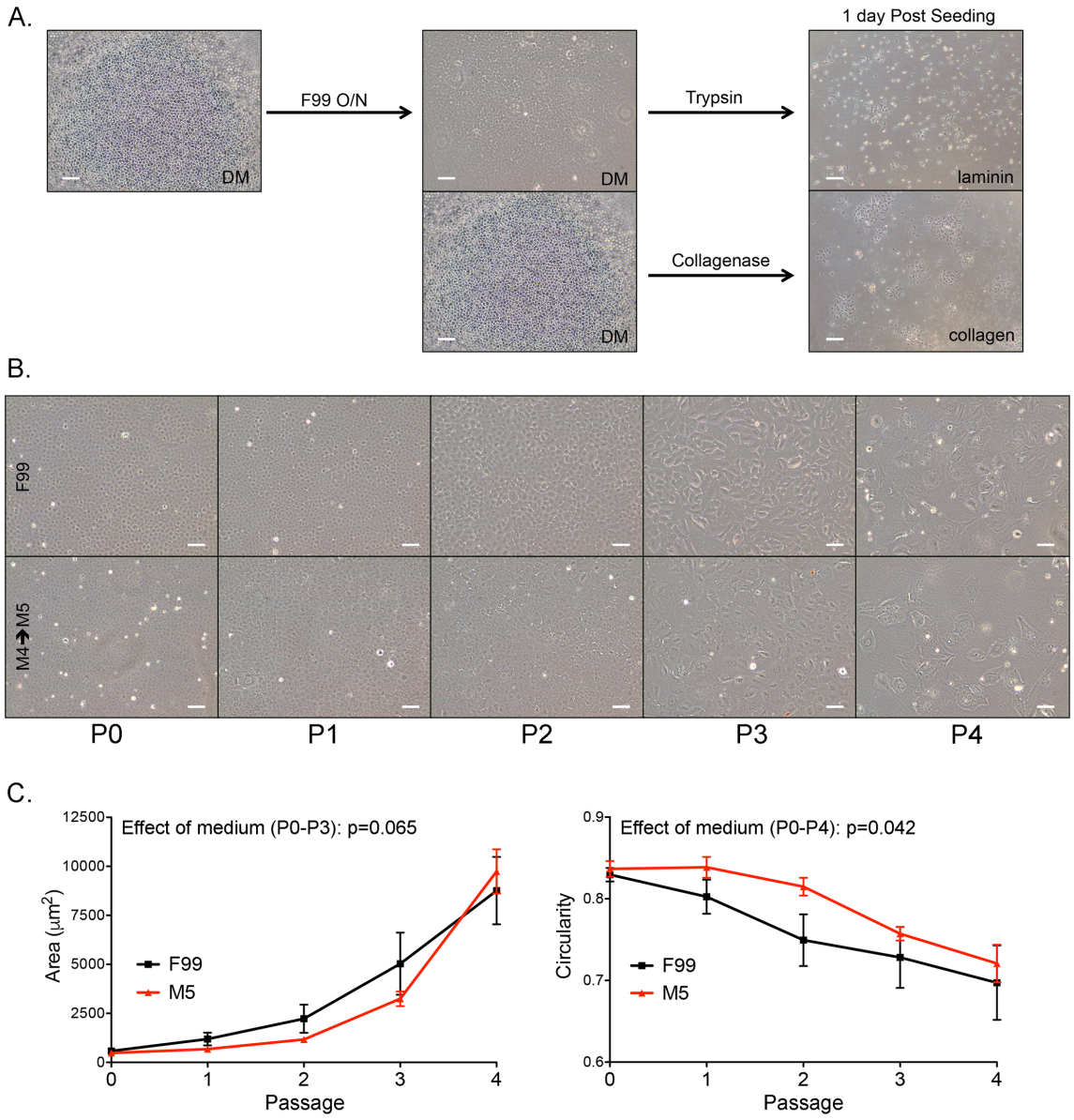

Figure 1. M5 medium delays morphologic features associated with a senescent phenotype. (A) Two protocols for the isolation and culture of primary CEnC. After detachment from the cornea, Descemet membrane (DM) with the attached endothelium was either incubated overnight in F99 medium at 37C (left panel) or subjected directly to collagenase digestion (middle panel). Cells incubated overnight were detached from DM with trypsin and seeded onto laminin-coated plastic. Cells dissociated from DM using collagenase were seeded onto collagen-coated plastic. Images show cells 1-day after seeding (right panel). (B) Images show confluent CEnC cultures at five passages using two culture methods (F99 or M5). (C) Line graph shows mean cell area (μm) at each passage. (D) Line graph shows mean circularity at each passage. Data in (C) and (D) are represented as the mean ±SEM (n=6). Statistical comparisons were performed using two-way ANOVA, with passage and medium defining the variables for this comparison. Scale bars, 100 μm.

255 **A low mitogenic environment maintains a robust CEnC-specific gene expression profile in primary**
256 **CEnC**

257 To examine the ability of the cultured cells to maintain a CEnC-specific gene expression profile in low-
258 or high-mitogenic environments, we compared the expression of 97 genes, previously identified as
259 specific to ex vivo corneal endothelium (evCEnC), in primary CEnC in M5 versus F99 at each passage
260 (Fig. 2) (Frausto et al., 2016). At P0, the cells in M5 expressed 83 of the 97 (85.6%) evCEnC-specific
261 genes, while cells in F99 expressed 76 (78.4%) (Fig. 2A). By P4, the percentages decreased to 75.3%
262 (73/97) in cells cultured in M5, and 66% (64/97) in cells cultured in F99 (Fig. 2A). We examined the 97
263 evCEnC-specific genes in the passaged cells to identify those that may be suitable positive selection
264 markers for assessing the quality of CEnC cultures using the following criteria: 1) expression in 2 or more
265 sequential passages, starting with P0; 2) decreasing expression over increasing passages (Fig. 2B); and 3)
266 encoding a cell surface protein. Only *TMEM178A* demonstrated these characteristics (Fig. 2C), and its
267 expression was validated by qPCR at P0 and P3 (Fig. 2D).

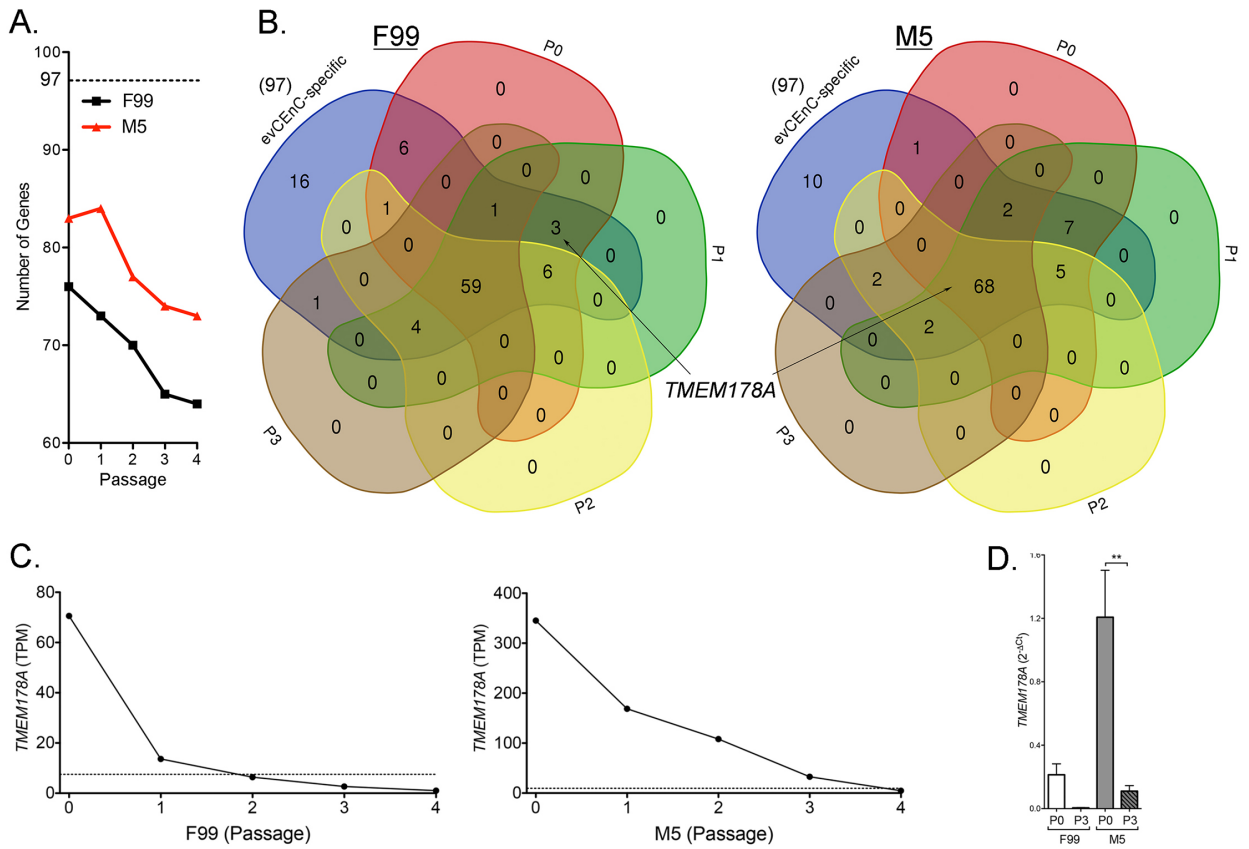

Figure 2. M5 medium maintains CEnC-specific gene expression in cultured CEnC. (A) Line graph shows the number of evCEnC-specific genes expressed in CEnC cultured in either F99 or M5 medium. Dashed line represents the number (97) of evCEnC-specific genes identified in a previous study. (B) Venn diagrams demonstrating the expression of evCEnC-specific genes at passages P0-P3 (P4 not shown due to difficulty visualizing Venn diagrams of greater than 5 sets). *TMEM178A* was identified as a cell surface marker expressed in early passages (at least P0 and P1) in CEnC cultured in either F99 or M5. (C) Line graphs show expression pattern of *TMEM178A* in CEnC cultured in F99 or M5. Gene was considered expressed if TPM value was greater than 7.5 (dashed line). (D) Bar graph shows *TMEM178A* transcript abundances in P0 and P3 CEnC using qPCR. Data in (D) are represented as the mean ±SEM (n=4). Statistical comparisons were performed using one-way ANOVA with post-hoc Tukey test. **, P<0.01.

An analysis of the expression of genes purported to be markers for CEnC identity and/or to determine the quality of CEnC in culture revealed that many were neither specific nor highly expressed in corneal endothelium (e.g., *ATP1A1*, *TJP1*, *VIM*, *PRDX6*, *SLC3A2*), or did not correlate well with other quality metrics, such as cell morphology (e.g., *ALCAM1*, *ERBB2*, *CD248*, *SLC25A11*)(Fig. S2). We should note that our data represents transcript abundance, and these markers may prove to be adequate based on protein abundance, but in our study we did not examine the majority of the reported markers for

287 protein abundance. Of these markers, we found that *SLC4A11* and *CD44* may represent the optimal
288 markers for selection of high quality cultured CEnC, with *SLC4A11* classified as a positive selection
289 marker and *CD44* classified as a negative selection marker (Fig. 3). *SLC4A11* and *CD44* transcript
290 abundances at P0 and P3 in CEnC cultured in both F99 and M5 was determined by RNA-seq and
291 validated by both qPCR and a Western assay (Fig. 3A). Expression of *SLC4A11*, which was high in
292 evCEnC, decreased with increasing passage, while expression of *CD44*, which was high in evCEpC,
293 increased with increasing passage (Fig. 3B).

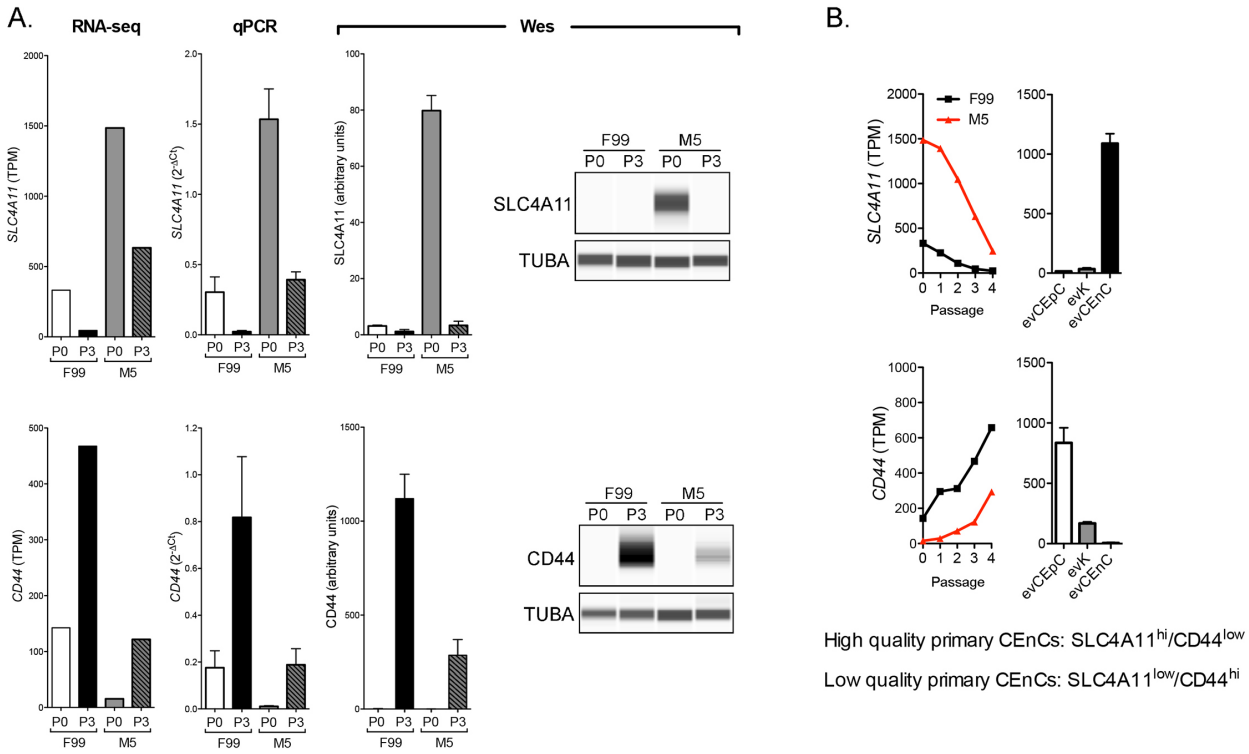

294

295 **Figure 3. SLC4A11 and CD44 as cell surface markers for the selection of high quality cultured**
296 **CEnC.** Assessment of previously published markers and results obtained in this study provide evidence
297 that SLC4A11 and CD44 represent the most informative markers for the selection of high quality cultured
298 cells, and represent a minimum for selection. (A) Bar graphs show transcript (RNA-seq and qPCR)
299 abundance of *SLC4A11* and *CD44* in P0 and P3 CEnC cultured in F99 and M5. Detection and
300 quantification of SLC4A11 and CD44 was performed using a Western assay (Wes). Bar graphs show
301 protein quantification. (B) Line graphs show *SLC4A11 and CD44* transcript quantities in CEnC at each
302 passage (P0 – P4). Bar graphs show transcript abundance in the three main cell types of the cornea
303 ((epithelial cells (evCEnC), keratocytes (evK) and endothelial cells (evCEnC)). Data in bar graphs in (A)
304 are represented as the mean ±SEM (n=4, mRNA; n=3, protein). Data in line graphs are represented as the
305 mean TPM at each passage (n=7). Data in bar graphs in (B) are represented as the mean TPM ,±SEM
306 (n=3).
307

CEnC grown in a low-mitogenic environment possess a robust cellular respiration phenotype

We performed bioinformatics analyses using differentially expressed genes to determine the biological characteristics of cells cultured with F99 and M5. We identified the genes that were significantly differentially expressed in cells at each passage between the two growth conditions (Table S4). With progressive passaging, the number of genes showing differential expression (M5 compared to F99 at each passage) decreased for cells in each media condition, with the transcriptomes of the cells grown in F99 and cells grown in M5 becoming increasingly more similar (Fig. S3A). As the gene expression difference was greatest at P0 (between F99 and M5), we performed bioinformatics analyses on the data set obtained at P0. The genes upregulated in cells with each media at P0 were subsequently analyzed to identify gene ontology (GO) and pathway terms enriched in our data sets (Table S5). GO terms significantly (q-value <0.05) enriched in the F99 (P0) upregulated genes data set were associated with cell differentiation and tissue development (e.g., developmental process, system development, and multicellular organism development)(Table 1). In addition, significantly enriched pathway terms were associated with cell state transitions (e.g., TGF-beta signaling pathway and epithelial to mesenchymal transition in colorectal cancer) and cell senescence (e.g., senescence and autophagy in cancer). The significantly enriched GO terms in the M5 (P0) upregulated genes data set were associated with cellular respiration (e.g., oxidoreductase activity and electron transfer activity) and lipid metabolism (e.g., lipid oxidation and fatty acid oxidation). Similarly, pathway terms enriched in this data set were also associated with cellular respiration (e.g., electron transport chain (OXPHOS system in mitochondria)) and lipid metabolism (e.g., fatty acid metabolism). GO and pathway enrichment results were similar for the other passages within the same media group (Table S5).

Senescence of primary CEnC is not dependent on mitogen concentration

To determine whether the observed senescent-associated morphogenic changes coincide with gene expression changes, we assessed the expression changes for genes previously associated with cell senescence (Table S6). Many of these genes demonstrated marked expression changes and trends in

334 expression that are consistent with the senescent phenotype observed for many distinct cell systems. To
335 determine the functional consequences of changes in gene expression, we identified genes that were
336 significantly differentially expressed at each passage (P0 was the reference), and for each medium (Table
337 S7). Passage 3 and 4 showed the greatest number of differentially expressed genes (Fig. S3B), which
338 coincided with marked changes in morphometric measures. We subsequently performed GO and pathway
339 analysis to determine the GO and pathway terms enriched in this data set (Table S8). GO terms
340 significantly (q-value<0.05) enriched in the F99 (P3 and P4) differentially expressed genes data set were
341 associated with cell senescence-associated GO terms (e.g., mitotic cell cycle, response to stress and
342 MAPK cascade), and enriched pathway terms also associated with senescence (e.g., p53 signaling
343 pathway and cellular senescence)(Table 2). Similarly, the significantly enriched GO and pathway terms in
344 the M5 (P3 and P4) differentially expressed genes data set were also associated with cellular senescence,
345 but showed significant enrichment for pathway terms associated with cellular energy processing (e.g.,
346 oxidative phosphorylation and the citric acid (TCA) cycle and respiratory electron transport).

347 The gene ontology and pathway analyses described above identified biological features in CEnC
348 as a consequence of differentially expressed genes. However, these analyses are performed in the absence
349 of the known direction of differential expression (i.e., downregulated and upregulated) for each gene. To
350 utilize the direction of differential gene expression for the purpose of informing not only pathway
351 enrichment, but also pathway activation state, we used the Ingenuity Pathway Analysis software (Table
352 S9). Significantly activated (z-score>1) pathways in all (P3 (F99 and M5) and P4 (F99 and M5)) data sets
353 were associated with an immune-like response (Table 3). Significantly deactivated (z-score<-1.0)
354 pathways for all data sets were generally associated with metabolic pathways, which included pathways
355 associated with lipid metabolism, nucleotide biosynthesis, glycolysis and cellular respiration.

356 Cell senescence is characterized by an irreversible cell cycle arrest. To determine the impact of
357 passaging (i.e., expansion) on the cell cycle, we examined the intra-media data sets by focusing on the
358 predicted activation state (as predicted by IPA software) of cell cycle functions (Table S10). Generally,
359 this analysis demonstrated activation (z-score>0.5) of cell senescence-associated functions (e.g.,

360 senescence of cells) and deactivation (z-score<-1.0) of cell cycle functions that have a positive effect on
361 the cell cycle (e.g., mitosis and cell and cell cycle progression) (Table 4).
362
363 **Senescence of primary CEnC involves the activation of the p53 and p38-MAPK pathways**
364 To determine whether senescence of primary CEnC involves activation of the p53 and p38-MAPK
365 pathways and regulation of the cell cycle, we examined expression and activation of genes/proteins
366 known to regulate cell cycle arrest due to senescence (Fig. 4). We created a custom pathway network that
367 included p53 (TP53) and p38-MAPK (MAPK14), the cyclin-dependent kinase inhibitors $p21^{CIP1}$
368 (CDKN1A) and $p16^{INK4}$ (CDKN2A), and well-established markers of cell senescence (LMNB1,
369 GADD45A and CD44) (Fig. 4A). In addition, we included the "senescence of cells" as the phenotype
370 connecting these factors. Initially, we superimposed the differential gene expression results (fold-change)
371 for genes encoding these proteins, and then we applied an algorithm that predicted the "activation" state
372 of the other proteins and the phenotype. Applying the prediction algorithm demonstrated activation of
373 both p53 and p38-MAPK, and activation of "senescence of cells" phenotype in primary CEnC at P3 in
374 both F99 and M5. Detection of phosphorylation of p53 and p38-MAPK at P3 by Western blotting
375 provided confirmation of their activation (Fig. 4B). Although *TP53* and *MAPK14* gene expression were
376 not markedly different between P0 and P3 CEnC, phosphorylation of the encoded proteins was
377 significantly greater at P3 than P0 ($p<0.05$)(Fig. 4C). In addition, significant ($p<0.05$) differential gene
378 expression of the senescence markers *LMNB1*, *GADD45A* and *CD44* was observed at P3 in either F99 or
379 M5 or both, a result consistent with cell senescence (Fig. 4D). In addition, we confirmed significantly
380 increased expression of the CD44 protein at P3, which was consistent with *CD44* transcript levels.

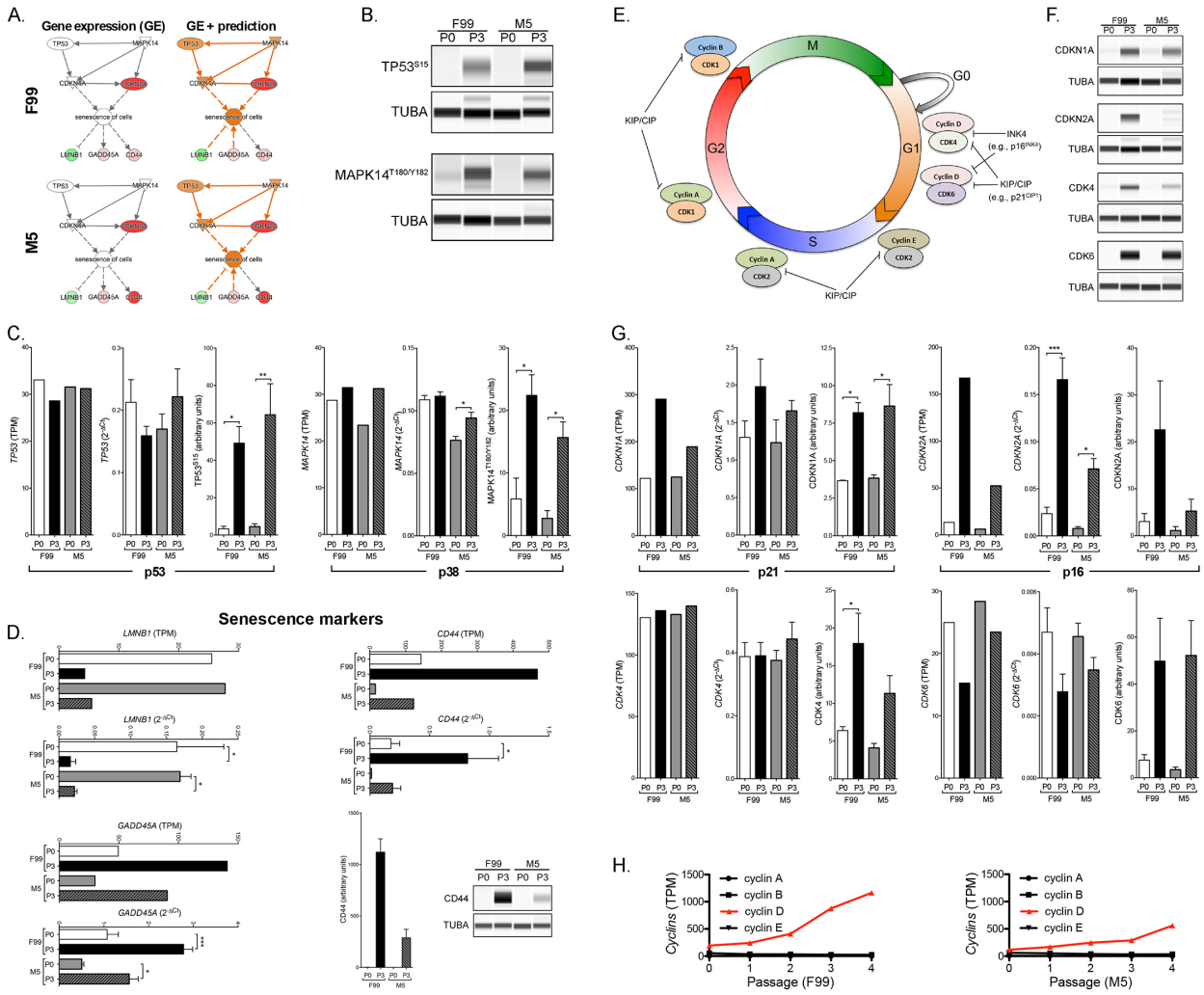

Figure 4. Cellular senescence of cultured CEnC is associated with activation of p53 and p38-MAPK pathways. (A) Classic cell senescence pathway involving p53 (TP53) and p38 (MAPK14). Pathway schematics show expression of senescence-associated genes that were differentially expressed in P3 CEnC (left panel). Shades of green, decreased expression; shades of red, increased expression. Pathway schematics show differentially expressed genes together with activity prediction results (orange, activated; blue, repressed) for upstream and downstream factors (right panel). (B) Western results show phosphorylation of TP53 at Serine 15 and MAPK14 at Threonine 180 and Tyrosine 182 in CEnC at P0 and P3, cultured in either F99 or M5. (C) Bar graphs show *TP53* and *MAPK14* transcript levels in P0 and P3 CEnC using RNA-seq and validated by qPCR. Bar graphs show the quantification of TP53 and MAPK14 phosphorylation in P0 and P3 CEnC. (D) Bar graphs show the transcript abundances of *LMNB1*, *GADD45A* and *CD44*, and validated using qPCR. Bar graphs show CD44 protein abundances detected using a Western assay. (E) Diagram of the cell cycle including factors that positively (cyclins and CDK) and negatively (INK4 and KIP/CIP) regulate cell cycle progression. (F) The $p21^{CIP1}$ (CDKN1A) and $p\ 16^{INK4}$ (CDKN2A) are inhibitors of cyclin-dependent kinases, and are classically associated with cellular senescence. Western results show increased expression of CDKN1A and CDKN2A concomitant with increased expression of the CDK4 and CDK6 in CEnC at P3, cultured in either F99 or M5. (G) Bar graphs show: *CDKN1A*, *CDKN2A*, *CDK4* and *CDK6* transcript levels in P0 and P3 CEnC using RNA-seq and validated by qPCR; the quantification of the proteins encoded by these genes in P0 and P3 CEnC. (H) Line graphs show the transcript abundances of the cyclins at each passage

401 in CEnC cultured in F99 or M5. TUBA was used as a loading control in the Westerns. Data in bar graphs
402 are represented as the mean ±SEM (n=4, mRNA; n=3, protein). Statistical comparisons were performed
403 using one-way ANOVA with post-hoc Tukey test. *, P<0.05; **, P<0.01; ***, P<0.001.
404
405 The cell cycle includes various phases (G1, S, G2 and M) that involve cyclin and cyclin-
406 dependent kinases (CDK) (Fig. 4E). In the absence of inhibitors of the CDK, cell cycle progression is
407 dependent on the availability and interaction of cyclins and CDK. However, two classes of inhibitors,
408 INK4 and KIP/CIP, are able to inhibit cell cycle progression via interaction of the inhibitors (e.g., $p21^{CIP1}$
409 and/or $p16^{INK4}$) with the cyclin/CDK complexes, an interaction that ultimately blocks the complexes'
410 downstream actions and results in cell cycle arrest. We assessed protein expression of both $p21^{CIP1}$
411 (CDKN1A) and $p16^{INK4}$ (CDKN2A), which are upregulated in senescent cells (Fig. 4F). Marked increases
412 in both of these inhibitors were observed in P3 CEnC cultured in F99 or M5. In addition, accumulation of
413 CDK4 and CDK6, CDK important in progression through G1/S of the cell cycle, was observed in P3 cells
414 cultured in F99 and M5 (Fig. 4F). While transcript quantification demonstrated a significant increase in
415 gene expression in P3 cells only for CDKN2A, the expression of the encoded proteins were either
416 significantly (p<0.05; CDKN1A, CDK4) or markedly (CDKN2A, CDK4 and CDK6) increased in P3
417 cells cultured in F99 and M5 (Fig. 4G)., As an increase in cyclin D, in conjunction with increases in
418 $p16^{INK}$ (CDKN2A), CDK4 and CDK6, is a hallmark of G1 cell cycle arrest, we measured the expression
419 of the four cyclins (cyclins A, B, D and E). A marked and progressive increase in cyclin D was observed
420 in cells cultured in both F99 and M5, in contrast to the expression of the other three cyclins, which was
421 unchanged through P4 (Fig. 4H).
422
423 **Low mitogenic conditions establish a robust functional barrier in CEnC**
424 To determine the impact of cell culture conditions on the establishment of a functional barrier, we
425 measured resistance of the CEnC to an electrical current (Fig. 5). Initially, we measured barrier function
426 of cells isolated/grown using unmodified protocols for each of the two methods employed in this study
427 (Tryp-LN-F99 and ColA-ColIV-M4M5) CEnC cultured using the ColA-ColIV-M4M5 method
428 demonstrated markedly greater impedance compared with CEnC cultured using the Tryp-LN-F99 method

429 (Fig. 5A). Impedance data was then used to model cell-cell (R_b) and cell-substrate (α) interactions, which
430 demonstrated that both contribute to the greater barrier function observed in cells cultured using the
431 ColA-ColIV-M4M5 method. To identify a potential effect of the dissociation enzymes (trypsin and
432 collagenase A) on the establishment of a functional barrier, we modified the isolation/growth protocols to
433 exchange one enzyme for the other. Exchanging the enzymes did not have a marked effect on the
434 establishment of a functional barrier, with the cells cultured using the protocol containing ColIV-M4M5
435 establishing a more robust functional barrier compared with cultures established with the protocol
436 containing LN-F99 (Fig. 5B). To determine the contribution, if any, of the substrate (laminin or collagen)
437 to which the cells adhere, or of the media (F99 or M5) in which the cells are cultured, we exchanged the
438 substrates for each other and used F99 and M5 for each (Fig. 5C). Due to the limitation in the number of
439 replicates we could assay, we chose trypsin (Tryp) as the dissociation enzyme, since use of either trypsin
440 or collagenase A did not make a significant difference on establishment of a functional barrier. While
441 only marginal differences in the electrical impedance were observed up to approximately 48 hours, after
442 that time point the cells that were cultured using the Tryp-LN-M4M5 method demonstrated a
443 progressively weakening barrier. Additionally, the cells that were cultured using the Tryp-LN-M4M5
444 method demonstrated a marked decrease in cell-cell and cell-substrate adhesion after 48 hours.

445 To determine whether the differences observed in barrier function between the two culturing
446 methods (F99 versus M5) could be explained by differences in barrier-associated proteins or in the
447 organization of the adhesive interactions between cells, we examined the expression and localization of
448 the cadherin protein CDH2. While *CDH2* transcript levels measured by qPCR were significantly ($p<0.01$)
449 lower in cells cultured in M5, the CDH2 protein levels were not different (Fig. 5D). However, the
450 organization of the adhesive interaction between cells was markedly different between cells grown in F99
451 and M5 (Fig. 5E). In F99, the cell-cell interactions appeared diffuse and frayed, although these features
452 were not consistent for all cell-cell interactions, and lacked features of a well-formed lateral membrane. In
453 contrast, the cells grown in M5 appeared to have consistent cell-cell interactions with what appears as
454 prominent lateral membranes, which give the image the impression of depth.

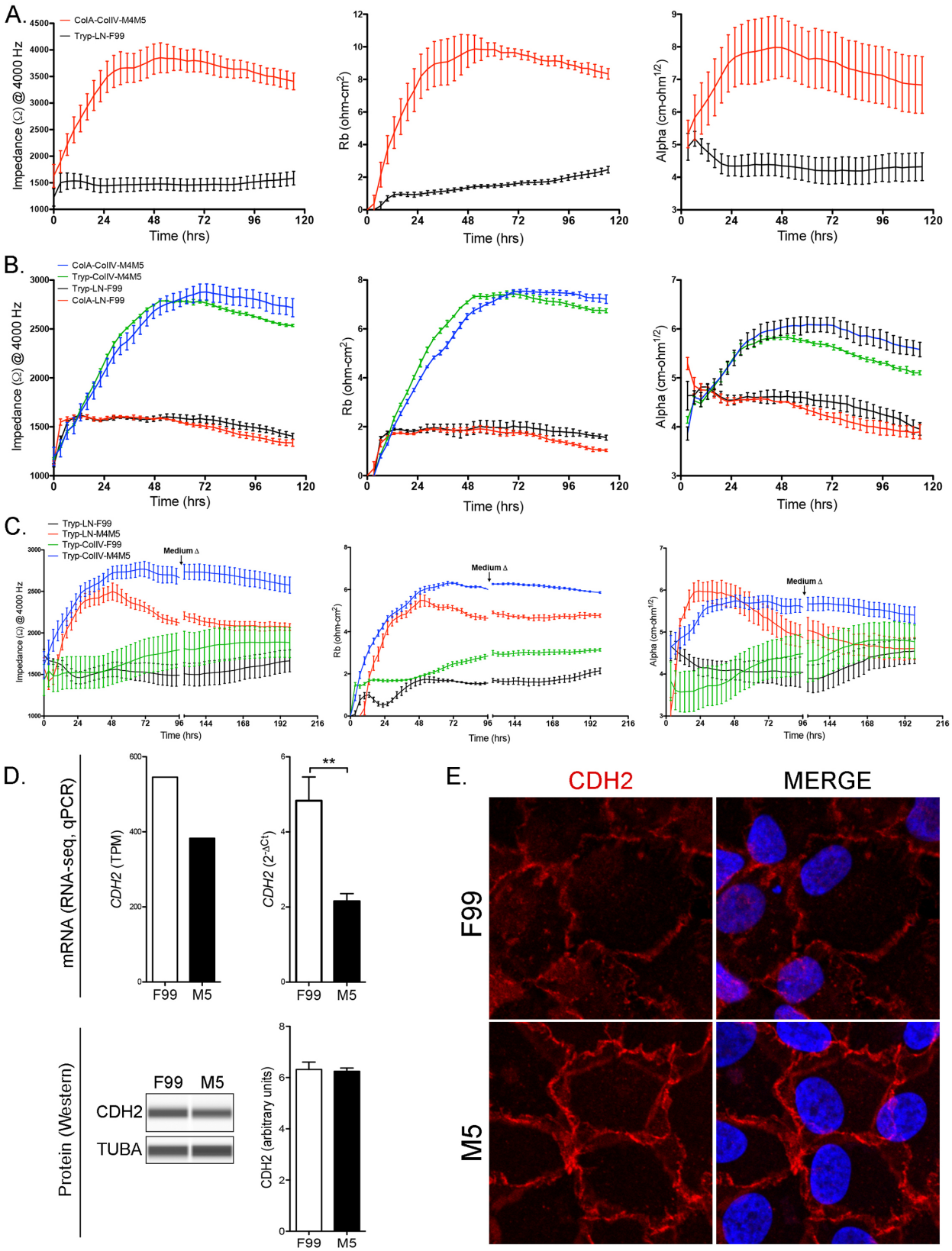
A.
ColA-ColIV-M4M5
Tryp-LN-F99
Impedance (Ω) @ 4000 Hz
Rb (ohm-cm²)
Alpha (cm-ohm^1/2)
Time (hrs)
B.
ColA-ColIV-M4M5
Tryp-ColIV-M4M5
Tryp-LN-F99
ColA-LN-F99
C.
Tryp-LN-F99
Tryp-LN-M4M5
Tryp-ColIV-F99
Tryp-ColIV-M4M5
Medium Δ
D.
mRNA (RNA-seq, qPCR)
CDH2 (TPM)
CDH2 (2^-ΔCt)
**
F99
M5
Protein (Western)
CDH2
TUBA
CDH2 (arbitrary units)
E.
CDH2
MERGE
F99
M5

455

456 **Figure 5. Cultured CEnC establish and maintain robust barrier function in M5 medium.** (A) Line
457 graph shows electrical impedance (Ω at 4000 Hz) for P0 CEnC monolayers established in F99 and M5
458 media. The contribution of cell-cell adhesion to the resistance of electrical current was modeled from
459 impedance data and given as R_b (Ω • cm^2). The contribution of cell-substrate adhesion to resistance of
460 electrical current was modeled from impedance data and given as (α, $\Omega^{½}$ • cm). (B) Line graph shows
461 electrical impedance for CEnC monolayers established from cells dissociated with trypsin (Tryp) or
462 collagenase (ColA), and each cultured in F99 and M5 medium. The contribution of cell-cell (R_b) and cell-
463 substrate (α) to electrical resistance were modeled from the impedance data. (C) Line graph shows
464 electrical impedance for CEnC monolayers established from cells dissociated with trypsin (Tryp), seeded
465 on either laminin (LN) or collagen (ColIV), and cultured in either F99 and M5 medium. The contribution
466 of cell-cell (R_b) and cell-substrate (α) to electrical resistance was modeled from the impedance data. (D)
467 Bar graphs show abundance of *CDH2*, a contributor to cell-cell adhesion, in CEnC cultured in F99 and
468 M5 (top panel). Western results for CDH2 protein and bar graph shows protein quantification (bottom
469 panel). TUBA was used as a loading control in the Western. (E) Immunofluorescence results show
470 localization of CDH2 protein in CEnC cultured in F99 and M5. Red, Alexafluor 594; blue, DAPI. Data in
471 line graphs are represented as the mean ±SD (n=4), and data in bar graphs are represented as the mean
472 ±SEM (n=4, mRNA; n=3, protein). Statistical comparisons were performed using one-way ANOVA with
473 post-hoc Tukey test. **, P<0.01.
474

475 **A strong functional barrier in primary CEnC is associated with robust expression of adhesion and**
476 **glycocalyx proteins**

477 To determine the extent to which barrier-associated proteins may be involved in the more robust
478 establishment of a functional barrier of CEnC in M5 media, we examined several proteins associated with
479 either cell-cell adhesion or glycocalyx formation (Fig. 6). We first measured the expression of genes that
480 encode adhesion-associated proteins (CLDN11, AJAP1, TMEM204 and TMEM178A), and quantified
481 protein levels for each (Fig. 6A). The expression of each of the four genes was higher in CEnC cultured in
482 M5 compared to F99, reaching statistical significance (p<0.05) for all four when measured at the
483 transcript level by qPCR, and for two (CLDN11 and TMEM178A) when measured at the protein level
484 (p<0.01). We then measured the expression of genes that encode glycocalyx-associated proteins (APOE,
485 MYOC, DCN, LUM and APOD), and quantified protein levels for each (Fig. 6B). Significantly (p<0.05)
486 higher transcript levels were observed for all five genes in CEnC cultured in M5, but only two of the
487 proteins (MYOC and APOD) demonstrated significantly higher levels. The APOE (p=0.05) and LUM
488 (p=0.14) proteins were markedly higher in M5, but did not achieve statistical significance. DCN did not
489 demonstrate a difference in protein levels between the two media. Of note, APOD is known to exist in

three forms (pre-modified, post-modified, and complexed), each of progressively greater molecular weight, all of which demonstrated significantly ($p<0.05$) higher expression in M5 compared with F99.

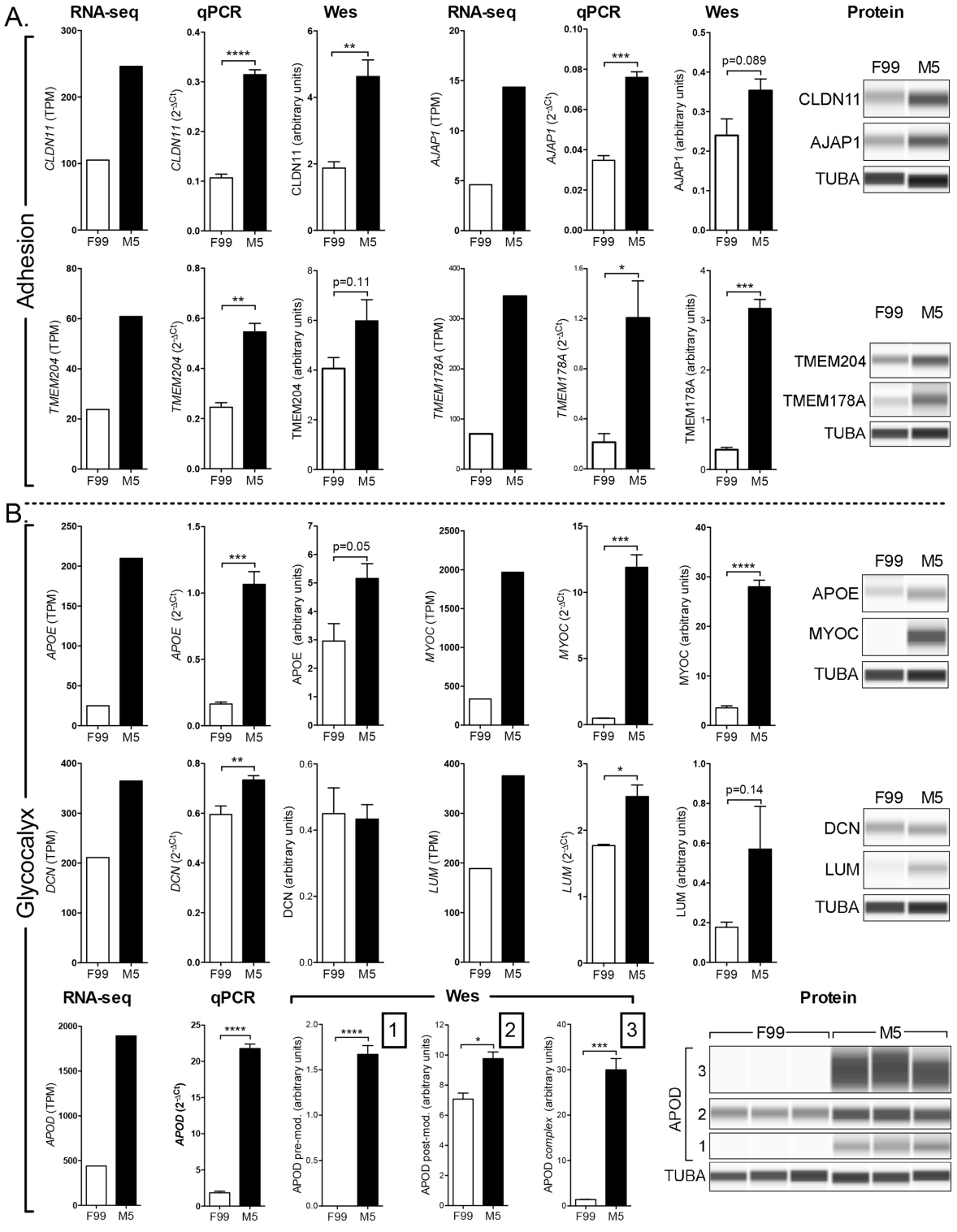

493 **Figure 6. M5 medium increases the expression of barrier-associated genes and proteins.** (A) Bar
494 graphs show the expression levels (RNA-seq and qPCR) of genes associated with cell adhesion
495 (*CLDN11*, *AJAP1*, *TMEM204* and *TMEM178A*) in P0 CEnC. Detection and quantification of the proteins
496 encoded by these genes were performed using a Western assay (Wes). (B) Bar graphs show the
497 expression levels (RNA-seq and qPCR) of genes associated with the glycocalyx (*APOE*, *MYOC*, *DCN*,
498 *LUM and APOD*). Detection and quantification of the proteins encoded by these genes were performed
499 using a Western assay (Wes). Three forms of APOD were observed, and each was quantified and
500 graphed. The protein forms observed were a pre-modified form (1), a post-modified form (2) and a high
501 molecular weight complex form (3). TUBA was used as a loading control in the Westerns. Data in bar
502 graphs are represented as the mean ±SEM (n=4, mRNA; n=3, protein). Statistical comparisons were
503 performed using one-way ANOVA with post-hoc Tukey test. *, P<0.05; **, P<0.01; ***, P<0.001; ****,
504 P<0.0001.
505

506 **Robust CEnC pump function is established by culture in low mitogenic conditions**

507 The SLC4A4, SLC4A11 and SLC16A1 transporters are highly expressed in in vivo corneal endothelium,
508 and play a prominent role in maintaining the solute gradients necessary for regulation of water transport
509 from the stroma to the anterior chamber. To determine the level of expression and functional capacity of
510 each in F99 and M5 media, we measured transcript levels by RNA-seq and qPCR, protein levels by
511 Western, and transporter activity with a fluorescence-based transporter assay (Fig. 7). *SLC4A11*
512 demonstrated significantly higher ($p<0.01$) and *SLC4A4* demonstrated non-significantly ($p=0.081$) higher
513 transcript levels in M5 medium, while the proteins encoded by all three genes demonstrated significantly
514 ($p<0.05$) higher levels in M5 compared with F99 (Fig. 7A).

515 To assess transporter function, we assayed for intracellular proton concentration (i.e., pH_i) over
516 time, including after changes in buffer perfusion, since each of the transporters transfer protons across the
517 plasma membrane (Fig. 7B). Traces showing intracellular pH demonstrate sensitivity to buffer changes
518 for each transporter. Qualitatively, the rate of change in intracellular proton concentration mediated by
519 SLC4A4 and SLC4A11 following a change in buffer appears greater in M5 compared with F99 medium.
520 In contrast, the rate of change in intracellular proton concentration mediated by SLC16A1 following a
521 change in buffer appears greater in F99 compared with M5 medium. Quantitatively, and as an indirect
522 measure of transporter activity, we calculated the change in intracellular proton concentration over time
523 ($d[H_i]/dt$) for each of the assays, and observed significantly ($p<0.01$) higher SLC4A4 and SLC4A11 and
524 significantly ($p<0.01$) lower activity for SLC16A1 for cells cultured in M5.

525

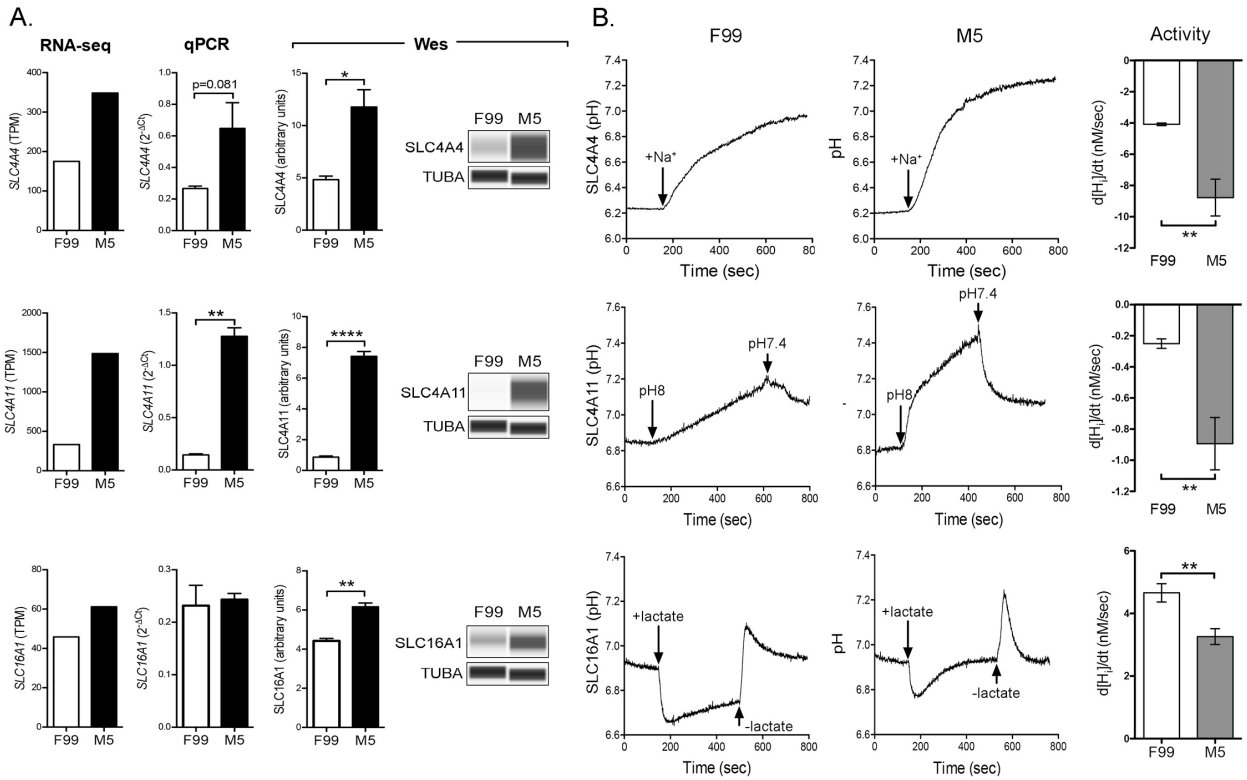

526

527 **Figure 7. SLC4A4 and SLC4A11 transporter activity is increased in M5 medium.** (A) Bar graphs
528 show transcript abundances (RNA-seq and qPCR) in P0 CEnC for genes that encode membrane bound
529 transporters (*SLC4A4*, *SLC4A11* and *SLC16A1*). Detection and quantification of the encoded proteins was
530 performed using a Western assay (Wes). (B) Traces show change in pH levels before and after perfusion
531 with buffer containing indicated substrate specified for the transporter (SLC4A4, Na^+; SLC4A11, H^+;
532 SLC16A1, lactate). Arrows indicate time at which buffer was changed. Bar graphs show the rate of
533 change in intracellular proton concentration [Hi], which was calculated as a proxy for transporter activity.
534 Data in bar graphs are represented as the mean ±SEM (n=4, mRNA; n=3, protein; n=6, transporter
535 activity). Statistical comparisons were performed using one-way ANOVA with post-hoc Tukey test. *,
536 P<0.05; **, P<0.01; ****, P<0.0001.
537

538 **Low mitogenic conditions cause decreased cell migration capacity**

539 We measured cell migration using a non-wounding method (Fig. 8). Phase contrast imaging of cell
540 migration demonstrated significantly (p<0.001) less gap closure for CEnC in M5 compared with F99
541 medium (Fig. 8A and B). We observed that cells cultured in M5, while possessing lower migration
542 capacity, also appear to markedly cover the gap primarily by increasing the cell size rather than by
543 migration (Fig. 8C). We calculated the ratio of the area occupied by the cells that "migrated" into the gap
544 versus cells more distant from the gap, and which have not substantially changed their size compared with

prior to when migration was initiated (Fig. 8D). Cell size for cells cultured in M5 and occupying any portion of the gap cover a significantly ($p<0.05$) larger area compared with cells cultured in F99.

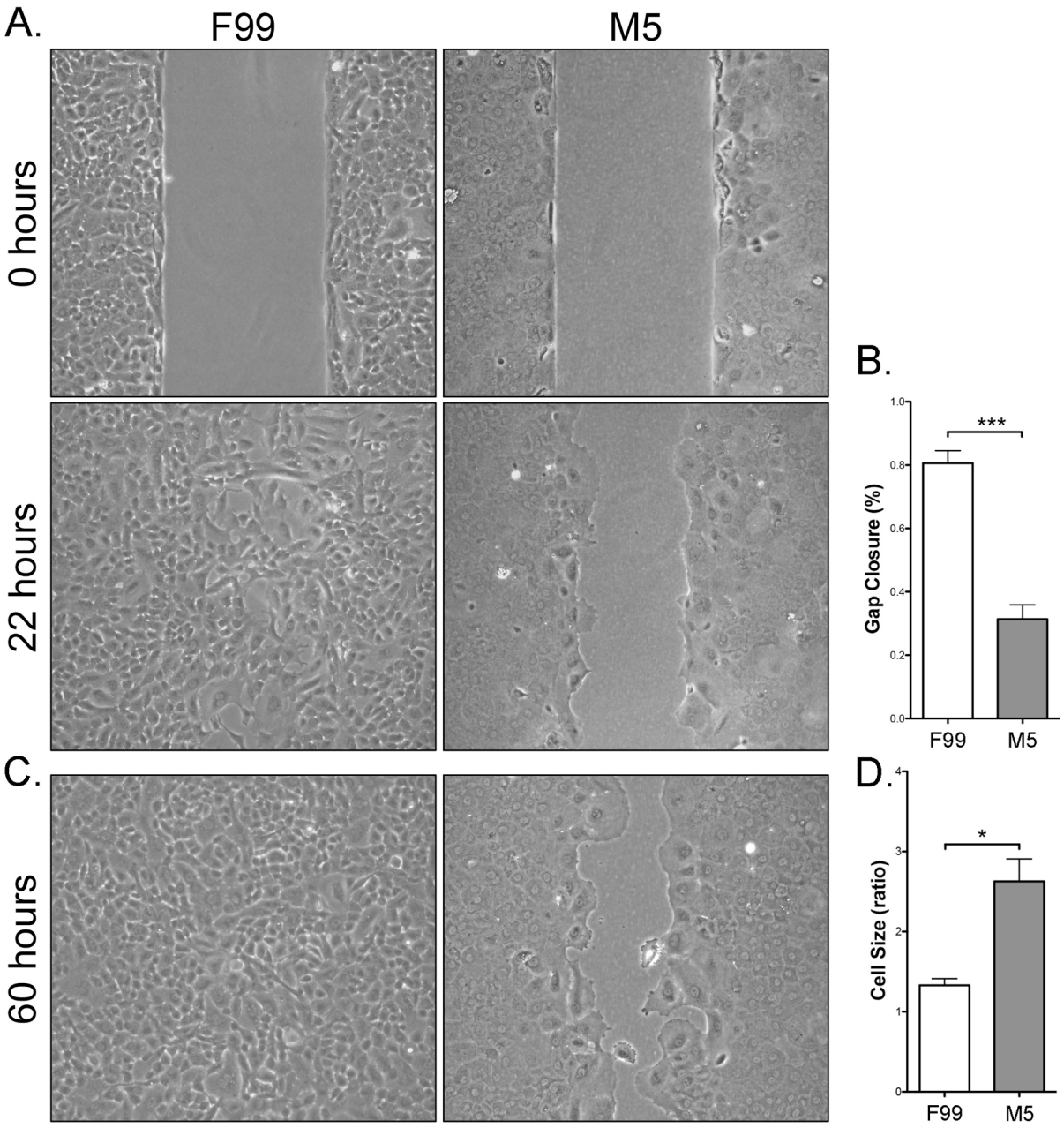

Figure 8. CEnC cultured in M5 medium possess attenuated migration capacity. (A) Phase contrast images show initial gap (0 hours) and gap closure (22 hours) of P0 CEnC cultured in F99 and M5. (B) Bar graph shows quantification of gap closure at 22 hours as a percent of the initial gap . (C) Phase contrast images show gap closure at 60 hours. (D) Bar graph shows the ratio of the mean area at 60 hours of the cells near or populating the gap divided by the mean area of the cells not near the gap. Data in bar graphs are represented as the mean ±SEM (n=4). Statistical comparisons were performed using one-way ANOVA with post-hoc Tukey test. *, $P<0.05$; ***, $P<0.001$.

556 **DISCUSSION**

557 Corneal clarity depends on the corneal endothelium, and disease or injury to this tissue causes loss of
558 visual acuity that may necessitate corneal transplantation. The development and widespread adoption of
559 endothelial keratoplasty techniques has significantly improved outcomes of the surgical management of
560 corneal endothelial cell dysfunction although postoperative complications remain (Deng et al., 2015; Lass
561 et al., 2017; Van den Bogerd et al., 2018). However, The current paradigm of one donor cornea for one
562 recipient requires cornea donation, recovery and utilization rates that are present in only a few countries
563 in the world that are able to meet the domestic need for transplantable corneas. Thus, scientist and
564 clinicians have developed various methods for isolation and in vitro culturing of CEnC, with the aim of
565 achieving sufficient cell numbers of transplantable high quality CEnC to challenge the one donor-one
566 recipient paradigm (Soh et al., 2017). While several metrics have been used to assess the identity (e.g.,
567 morphology, biomarker expression) and function (e.g., transcellular resistance, intracellular proton
568 concentration) and of cultured CEnC, a comprehensive study of the effects of in vitro expansion on the
569 CEnC transcriptome has not been performed. The transcriptomic work performed as part of this study
570 may be used as one of the criteria for assessing the quality and viability of in vitro expanded CEnC for
571 use in cell-replacement therapy. In particular, because cell senescence is a feature of primary cell culture,
572 it is important to identify all the potential signaling and metabolic pathways involved in CEnC senescence
573 in the hope of delaying senescence by targeting these pathways, and therefore producing a larger number
574 of therapeutically suitable cells.

575 In 1978, the first human CEnC cultures were described, but given a lack of human-specific
576 protocols, the researchers used culture conditions optimized for growth of rabbit CEnC (Jumblatt et al.,
577 1978). Over the next decade, techniques for the isolation of human CEnC and growth media for the in
578 vitro culture of human CEnC were optimized. In 1989, Engelmann et al. determined that a 1:1 mixture of
579 M199 and F12 media was the optimal base medium for culture of primary CEnC (Engelmann and Friedl,
580 1989). Two decades later, the formulation of the medium was modified to induce cell cycle re-entry (due
581 to relatively mitogen-rich conditions) and establishment of contact inhibition, leading to quiescence, a

582 non-proliferative cell state that characterize CEnC in vivo (Valtink et al., 2008). We started culturing
583 primary CEnC in 2011, and chose the medium formulation described by Valtink et al. as it was at the time
584 the most effective formulation for the culture of both primary and immortalized CEnC. Nevertheless,
585 about 40% (3/7 at P0 in this study) of the cultures we established did not possess CEnC-like morphology,
586 and were generally characterized by a mixture of morphologies (some resembling fibroblasts), an
587 observation consistent with previous findings by the developers of the formulation (personal
588 communication). In 2015, Peh et al. described a novel approach to in vitro culturing of CEnC in which
589 cell proliferation was accomplished by growth in a mitogenic-rich medium, followed by maintenance in a
590 medium with reduced mitogens (Peh et al., 2015). Coincidently, a recent report independently
591 demonstrated the superiority of the dual media approach (Bartakova et al., 2018). Taken together, these
592 studies indicated that the low mitogenic medium established cultures with better morphology, marker
593 expression and function compared with growth in a mitogen-rich medium alone. Herein, we compared the
594 two culture methods published by Valtnik et al. and Peh et al. using extensive bioinformatics analyses and
595 additional functional techniques to determine which method performs best in maintaining the CEnC
596 phenotype throughout in vitro expansion.

597 Cell morphology is an initial metric for assessing the quality of CEnC cultures. We observed that
598 the low mitogenic environment was better at maintaining a CEnC-like morphology, but continued
599 passaging caused a distinct morphogenic transformation consistent with cellular senescence. This change
600 in morphology correlated with a progressive loss of CEnC identity as defined by the expression of
601 evCEnC-specific genes. Temporal changes in evCEnC-specific gene expression as a consequence of
602 passaging allowed us to identify a novel cell surface marker, encoded by *TMEM178A*, as a potential
603 positive selection marker for high quality cultured CEnC. In addition, after a reassessment of reported
604 selection markers, we propose SLC4A11 (positive), TMEM178A (positive) and CD44 (negative) as the
605 minimum for selection of high quality in vitro CEnC (Bartakova et al., 2018; Cheong et al., 2013; Chng et
606 al., 2013; Ding et al., 2014; Frausto et al., 2016; Okumura et al., 2014a; Toda et al., 2017; Yoshihara et
607 al., 2015). SLC4A11 is a highly expressed transporter protein in corneal endothelium that plays a

608 significant role in CEnC function, and biallelic mutation of this protein leads to congenital hereditary
609 endothelial dystrophy (Aldave et al., 2013; Jiao et al., 2007; Vithana et al., 2006). Conversely, CD44 is
610 not expressed in the corneal endothelium, and its expression correlates with a senescent phenotype in
611 vascular and corneal endothelial cells (Mun and Boo, 2010; Ueno et al., 2016).

612 A prominent barrier to expansion of CEnC in vitro for use in a cell-based therapy is the limited
613 proliferative capacity of primary CEnC. In vivo, CEnC are in a state of cellular quiescence, which in this
614 cell type is specifically a cell cycle arrest at the G1 phase that is established by contact-inhibition,
615 maintained by TGFβ2, and regulated by $p27^{KIP1}$ (Joyce, 2003). However, in vivo CEnC have been shown
616 to express senescent markers in older donors, which is postulated to contribute to the lower proliferative
617 capacity of primary CEnC isolated from older donors compared with those from younger donors.
618 Nevertheless, CEnC are able to re-engage the cell cycle by loosening of cell-cell contacts and/or exposure
619 to potent mitogenic factors. As with most primary cells, primary CEnC have a limited life span under
620 proliferative (i.e., passaging and growth in mitogen-rich) conditions. This limitation is caused by cellular
621 senescence of CEnC (in vitro and ex vivo), and may be, in part, a consequence of oxidative stress (Joyce
622 et al., 2009). This is supported by our observations in late passage CEnC (P3 and/or P4) that p38MAPK
623 was phosphorylated (stress response), that expression of $p16^{INK4}$ (gene and protein) was increased, and
624 that the set of differentially expressed genes was enriched for genes implicated in oxidative stress-
625 associated pathways (e.g., NRF2-mediated oxidative stress response, DNA damage checkpoint
626 regulation). In addition, there is also an apparent repression of oxidative phosphorylation (i.e.,
627 mitochondrial activity), which was observed in our pathway analysis. Moreover, we also identified
628 enrichment for genes associated with p53 signaling, an observation made previously (Sheerin et al.,
629 2012), and this coincided with phosphorylation of p53 and increased expression of $p21^{CIP1}$ (CDKN1A)
630 (gene and protein) in senescent CEnC (i.e., P3 and P4). Cell senescence in primary CEnC in this study
631 was also associated with increased expression of CDK4 and CDK6 proteins (but not gene expression),
632 and increased *cyclin D* (*CCND1*) gene expression. Taken together, this represents a gene/protein
633 expression profile consistent with senescence-induced G1 cell cycle arrest. Overall, activation of the

634 p38MAPK and p53 pathways did not appear significantly influenced by growth in a low- or high-
635 mitogenic environment.

636 Achieving and maintaining characteristic CEnC functional properties is essential for the clinical
637 utility of in vitro CEnC in management of CEnC dysfunction. The corneal endothelium is a monolayer
638 mosaic of CEnC, and its primary function is to maintain the corneal stroma in a partially dehydrated state
639 to preserve its optical clarity. It does this by establishing a robust barrier conferred by cell-cell and cell-
640 substrate interactions, which allow for passive leak of water into the stroma, but not most solutes
641 (Srinivas, 2010). Through the combined action of various solute transporters, unidirectional translocation
642 of water from the stroma into the aqueous humor occurs (Bonanno, 2012). Taken together, this describes
643 the "pump-leak" hypothesis of water homeostasis in the cornea. We demonstrated that a low mitogenic
644 environment combined with culture on collagen represented better in vitro conditions for establishing a
645 robust CEnC barrier (as measured by electrical impedance) compared with a high mitogenic environment
646 and culture on laminin. Recent studies showed that collagen, compared with various other extracellular
647 matrix proteins, including laminin, and low mitogen-containing media were optimal for establishing
648 robust barrier function in a CEnC line (Santander-Garcia et al., 2016) and primary CEnC (Bartakova et
649 al., 2018). Detection of CDH2, a CEnC-specific marker, in CEnC cultures in low mitogenic conditions
650 demonstrated that cell adhesions (cell-cell and cell-substrate) are considerably more complex, and showed
651 striking resemblance to the organization of adhesions in ex vivo human corneas (He et al., 2016). We also
652 demonstrated that this increase in barrier function is associated with an increase in adhesion/glycocalyx-
653 associated protein expression. To our knowledge, this represents the first report implicating glycocalyx
654 proteins in corneal endothelial biology. Although some of the barrier-associated proteins we examined in
655 this study have been associated with the glycocalyx of the vascular endothelium (Friden et al., 2011;
656 Reitsma et al., 2007), it remains to be determined if the increase in glycocalyx-associated proteins
657 coincides with the formation of a glycocalyx in corneal endothelium either in vitro or in vivo. However,
658 early reports suggest that the human corneal endothelium may possess a glycocalyx-like layer composed
659 polysaccharides, glycosaminoglycans and other, as yet, unidentified molecules (Hornung and Wollensak,

660 1979; Jacobsen and Sperling, 1978; Schroder and Sperling, 1977; Sperling and Jacobsen, 1980). We also
661 showed that at least two transporters critical for CEnC function (SLC4A4 and SLC4A11) are expressed at
662 significantly higher levels and show increased transporter activity in low mitogenic conditions compared
663 with high mitogenic conditions. As such, CEnC expanded in mitogenic-rich medium and maintained in
664 low mitogenic conditions show functional features consistent with the CEnC requirement for regulating
665 water homeostasis in the cornea. These results are consistent with previous studies demonstrating an
666 intact pump function (i.e., prevention/mitigation of edema) in in vitro expanded corneal endothelial cells
667 in an animal model of bullous keratopathy (Peh et al., 2017; Peh et al., 2019).

668 A long known characteristic of in vivo CEnC is that when mild cell loss occurs, the vacated area
669 is covered by migration and increase in size of adjacent cells (Sherrard, 1976). To determine if this
670 phenomenon is recapitulated in vitro, we performed a non-wounding cell migration assay. Cells in a high
671 mitogenic environment migrated and/or proliferated (not distinguished in our study) to cover the gap with
672 no significant increase in cell size. In contrast, CEnC in low mitogenic conditions behaved in a manner
673 consistent with their behavior in vivo, so that these cells showed low migration capacity, but a significant
674 propensity to increase cell size to cover the gap. In addition, these results are consistent with the
675 differences observed for cell barrier formation, because increased cell-cell adhesion is antithetical to
676 robust cell migration (and also to robust cell proliferation capacity).

677 In summary, we provide evidence that CEnC proliferation in a high mitogenic medium, followed
678 by maintenance of contact-inhibition of confluent monolayers in a low mitogenic medium, supports
679 establishment of CEnC in which in vivo function is significantly recapitulated and permits sufficient
680 expansion of CEnC to significantly challenge the "one donor-one recipient" paradigm. In our current
681 study, we can theoretically achieve a 1:5-1:15 donor:recipient ratio (donor:recipient, 1:5 (P0) or 1:15 (P1)
682 – at approximately 3000 cells/mm^2), as these are the passages at which the cells possess the most robust
683 CEnC phenotype as determined by gene (or marker) expression and cell morphology. Maintaining the
684 CEnC morphologic and functional phenotype at higher passage numbers remains an active area of
685 research. Also, while we examined cell function at an early passage (typically at P0), we recognize that

686 functional analysis of cells will need to be performed at later passages to ensure viability as a therapeutic
687 modality. The progression to senescence in vitro remains a significant barrier to the expansion of
688 cultured CEnC. Identification of oxidative stress as a component of CEnC senescence has prompted
689 investigators to use p38MAPK inhibitors to delay the onset of senescence, but this approach has shown
690 mixed results (Hongo et al., 2017; Nakahara et al., 2018; Sheerin et al., 2012). Similarly, ascorbic acid
691 was a supplement added to early media formulations (added to F99 and M4) to reduce/inhibit oxidant-
692 induced stress/apoptosis (Serbecic and Beutelspacher, 2005; Shima et al., 2011). In addition, senescent
693 CEnC in vitro are characterized by the Senescence-Associated Secretory Phenotype (SASP), which
694 includes the secretion of immune-regulating factors (cytokines, chemokines and growth factors) that have
695 been demonstrated to support tumorigenesis in adjacent epithelial tissues (Georgilis et al., 2018; Laberge
696 et al., 2015; Lau and David, 2019; Lopes-Paciencia et al., 2019). As a remedy to senescence, we identify
697 both classical and novel pathways associated with CEnC senescence that can be manipulated
698 experimentally to potentially achieve significant CEnC expansion with minimal senescence. In addition,
699 we identified which previously reported markers represent the optimal markers for selection of high
700 quality cultured CEnC, and propose *TMEM178A* as a novel positive selection marker. We propose that
701 because senescent CEnC can be present in cultured CEnC preparations and that senescent cells may
702 support tumorigenesis, a Descemet membrane biomimetic carrier is preferred to injection of a suspension
703 of cells, to both maximize cell count and minimize their tumorigenic potential (Gutermuth et al., 2019;
704 Kinoshita et al., 2018; Teichmann et al., 2013). In conclusion, while additional changes to the dual media
705 method may improve the culturing of CEnC in vitro, we provide evidence that this method is preferred to
706 continuous culture in mitogen-rich media.

707 **REFERENCES**

708 Eye Bank Association of America. 2018 Eye Banking Statistical Report. 2018.

709 Aldave, A.J., Han, J., and Frausto, R.F. (2013). Genetics of the corneal endothelial dystrophies: an
710 evidence-based review. Clin Genet *84*, 109-119.

711 Baratz, K.H., Tosakulwong, N., Ryu, E., Brown, W.L., Branham, K., Chen, W., Tran, K.D., Schmid-
712 Kubista, K.E., Heckenlively, J.R., Swaroop, A., Abecasis, G., Bailey, K.R., and Edwards, A.O. (2010).
713 E2-2 protein and Fuchs's corneal dystrophy. N Engl J Med *363*, 1016-1024.

714 Bartakova, A., Kuzmenko, O., Alvarez-Delfin, K., Kunzevitzky, N.J., and Goldberg, J.L. (2018). A Cell
715 Culture Approach to Optimized Human Corneal Endothelial Cell Function. Invest Ophthalmol Vis Sci *59*,
716 1617-1629.

717 Bednarz, J., Rodokanaki-von Schrenck, A., and Engelmann, K. (1998). Different characteristics of
718 endothelial cells from central and peripheral human cornea in primary culture and after subculture. In
719 Vitro Cell Dev Biol Anim *34*, 149-153.

720 Bonanno, J.A. (2012). Molecular mechanisms underlying the corneal endothelial pump. Exp Eye Res *95*,
721 2-7.

722 Bray, N.L., Pimentel, H., Melsted, P., and Pachter, L. (2016). Near-optimal probabilistic RNA-seq
723 quantification. Nat Biotechnol *34*, 525-527.

724 Campisi, J. (2013). Aging, cellular senescence, and cancer. Annu Rev Physiol *75*, 685-705.

725 Cheong, Y.K., Ngoh, Z.X., Peh, G.S., Ang, H.P., Seah, X.Y., Chng, Z., Colman, A., Mehta, J.S., and Sun,
726 W. (2013). Identification of cell surface markers glypican-4 and CD200 that differentiate human corneal
727 endothelium from stromal fibroblasts. Invest Ophthalmol Vis Sci *54*, 4538-4547.

728 Chng, Z., Peh, G.S., Herath, W.B., Cheng, T.Y., Ang, H.P., Toh, K.P., Robson, P., Mehta, J.S., and
729 Colman, A. (2013). High throughput gene expression analysis identifies reliable expression markers of
730 human corneal endothelial cells. PLoS One *8*, e67546.

731 Deng, S.X., Sanchez, P.J., and Chen, L. (2015). Clinical outcomes of Descemet membrane endothelial
732 keratoplasty using eye bank-prepared tissues. Am J Ophthalmol *159*, 590-596.

733 Ding, V., Chin, A., Peh, G., Mehta, J.S., and Choo, A. (2014). Generation of novel monoclonal antibodies
734 for the enrichment and characterization of human corneal endothelial cells (hCENC) necessary for the
735 treatment of corneal endothelial blindness. MAbs *6*, 1439-1452.

736 Engelmann, K., and Friedl, P. (1989). Optimization of culture conditions for human corneal endothelial
737 cells. In Vitro Cell Dev Biol *25*, 1065-1072.

738 Frausto, R.F., Le, D.J., and Aldave, A.J. (2016). Transcriptomic Analysis of Cultured Corneal Endothelial
739 Cells as a Validation for Their Use in Cell Replacement Therapy. Cell Transplant *25*, 1159-1176.

740 Friden, V., Oveland, E., Tenstad, O., Ebefors, K., Nystrom, J., Nilsson, U.A., and Haraldsson, B. (2011).
741 The glomerular endothelial cell coat is essential for glomerular filtration. Kidney Int *79*, 1322-1330.

742 Georgilis, A., Klotz, S., Hanley, C.J., Herranz, N., Weirich, B., Morancho, B., Leote, A.C., D'Artista, L.,
743 Gallage, S., Seehawer, M., Carroll, T., Dharmalingam, G., Wee, K.B., Mellone, M., Pombo, J., Heide, D.,
744 Guccione, E., Arribas, J., Barbosa-Morais, N.L., Heikenwalder, M., Thomas, G.J., Zender, L., and Gil, J.
745 (2018). PTBP1-Mediated Alternative Splicing Regulates the Inflammatory Secretome and the Pro-
746 tumorigenic Effects of Senescent Cells. Cancer Cell *34*, 85-102 e109.

747 Gottsch, J.D., Bowers, A.L., Margulies, E.H., Seitzman, G.D., Kim, S.W., Saha, S., Jun, A.S., Stark,
748 W.J., and Liu, S.H. (2003). Serial analysis of gene expression in the corneal endothelium of Fuchs'
749 dystrophy. Invest Ophthalmol Vis Sci *44*, 594-599.

750 Gutermuth, A., Maassen, J., Harnisch, E., Kuhlen, D., Sauer-Budge, A., Skazik-Voogt, C., and
751 Engelmann, K. (2019). Descemet's Membrane Biomimetic Microtopography Differentiates Human
752 Mesenchymal Stem Cells Into Corneal Endothelial-Like Cells. Cornea *38*, 110-119.

753 He, Z., Forest, F., Gain, P., Rageade, D., Bernard, A., Acquart, S., Peoc'h, M., Defoe, D.M., and Thuret,
754 G. (2016). 3D map of the human corneal endothelial cell. Sci Rep *6*, 29047.

755 Hongo, A., Okumura, N., Nakahara, M., Kay, E.P., and Koizumi, N. (2017). The Effect of a p38
756 Mitogen-Activated Protein Kinase Inhibitor on Cellular Senescence of Cultivated Human Corneal
757 Endothelial Cells. Invest Ophthalmol Vis Sci *58*, 3325-3334.

758 Hornung, M., and Wollensak, J. (1979). [Proof of glycosaminoglycans in the corneal endothelium].
759 Albrecht Von Graefes Arch Klin Exp Ophthalmol *211*, 67-84.

760 Jacobsen, S.R., and Sperling, S. (1978). Scanning electron microscopic observations of a
761 mucopolysaccharide coating on human corneal endothelium. Acta Ophthalmol (Copenh) *56*, 161-167.

762 Jiao, X., Sultana, A., Garg, P., Ramamurthy, B., Vemuganti, G.K., Gangopadhyay, N., Hejtmancik, J.F.,
763 and Kannabiran, C. (2007). Autosomal recessive corneal endothelial dystrophy (CHED2) is associated
764 with mutations in SLC4A11. J Med Genet *44*, 64-68.

765 Joyce, N.C. (2003). Proliferative capacity of the corneal endothelium. Prog Retin Eye Res *22*, 359-389.

766 Joyce, N.C. (2005). Cell cycle status in human corneal endothelium. Exp Eye Res *81*, 629-638.

767 Joyce, N.C., Zhu, C.C., and Harris, D.L. (2009). Relationship among oxidative stress, DNA damage, and
768 proliferative capacity in human corneal endothelium. Invest Ophthalmol Vis Sci *50*, 2116-2122.

769 Jumblatt, M.M., Maurice, D.M., and McCulley, J.P. (1978). Transplantation of tissue-cultured corneal
770 endothelium. Invest Ophthalmol Vis Sci *17*, 1135-1141.

771 Kao, L., Azimov, R., Shao, X.M., Frausto, R.F., Abuladze, N., Newman, D., Aldave, A.J., and Kurtz, I.
772 (2016). Multifunctional ion transport properties of human SLC4A11: comparison of the SLC4A11-B and
773 SLC4A11-C variants. Am J Physiol Cell Physiol *311*, C820-C830.

774 Kinoshita, S., Koizumi, N., Ueno, M., Okumura, N., Imai, K., Tanaka, H., Yamamoto, Y., Nakamura, T.,
775 Inatomi, T., Bush, J., Toda, M., Hagiya, M., Yokota, I., Teramukai, S., Sotozono, C., and Hamuro, J.
776 (2018). Injection of Cultured Cells with a ROCK Inhibitor for Bullous Keratopathy. N Engl J Med *378*,
777 995-1003.

Krafchak, C.M., Pawar, H., Moroi, S.E., Sugar, A., Lichter, P.R., Mackey, D.A., Mian, S., Nairus, T., Elner, V., Schteingart, M.T., Downs, C.A., Kijek, T.G., Johnson, J.M., Trager, E.H., Rozsa, F.W., Mandal, M.N., Epstein, M.P., Vollrath, D., Ayyagari, R., Boehnke, M., and Richards, J.E. (2005). Mutations in TCF8 cause posterior polymorphous corneal dystrophy and ectopic expression of COL4A3 by corneal endothelial cells. Am J Hum Genet *77*, 694-708.

Laberge, R.M., Sun, Y., Orjalo, A.V., Patil, C.K., Freund, A., Zhou, L., Curran, S.C., Davalos, A.R., Wilson-Edell, K.A., Liu, S., Limbad, C., Demaria, M., Li, P., Hubbard, G.B., Ikeno, Y., Javors, M., Desprez, P.Y., Benz, C.C., Kapahi, P., Nelson, P.S., and Campisi, J. (2015). MTOR regulates the pro-tumorigenic senescence-associated secretory phenotype by promoting IL1A translation. Nat Cell Biol *17*, 1049-1061.

Lass, J.H., Benetz, B.A., Verdier, D.D., Szczotka-Flynn, L.B., Ayala, A.R., Liang, W., Aldave, A.J., Dunn, S.P., McCall, T., Mian, S.I., Navarro, L.C., Patel, S.V., Pramanik, S., Rosenwasser, G.O., Ross, K.W., Terry, M.A., Kollman, C., Gal, R.L., Beck, R.W., and Cornea Preservation Time Study, G. (2017). Corneal Endothelial Cell Loss 3 Years After Successful Descemet Stripping Automated Endothelial Keratoplasty in the Cornea Preservation Time Study: A Randomized Clinical Trial. JAMA Ophthalmol *135*, 1394-1400.

Lau, L., and David, G. (2019). Pro- and Anti-Tumorigenic Functions of the Senescence-Associated Secretory Phenotype. Expert Opin Ther Targets.

Livak, K.J., and Schmittgen, T.D. (2001). Analysis of relative gene expression data using real-time quantitative PCR and the 2(-Delta Delta C(T)) Method. Methods *25*, 402-408.

Lopes-Paciencia, S., Saint-Germain, E., Rowell, M.C., Ruiz, A.F., Kalegari, P., and Ferbeyre, G. (2019). The senescence-associated secretory phenotype and its regulation. Cytokine *117*, 15-22.

Mehta, J.S., Kocaba, V., and Soh, Y.Q. (2019). The future of keratoplasty: cell-based therapy, regenerative medicine, bioengineering keratoplasty, gene therapy. Curr Opin Ophthalmol *30*, 286-291.

Mimura, T., and Joyce, N.C. (2006). Replication competence and senescence in central and peripheral human corneal endothelium. Invest Ophthalmol Vis Sci *47*, 1387-1396.

Mun, G.I., and Boo, Y.C. (2010). Identification of CD44 as a senescence-induced cell adhesion gene responsible for the enhanced monocyte recruitment to senescent endothelial cells. Am J Physiol Heart Circ Physiol *298*, H2102-2111.

Nakahara, M., Okumura, N., Nakano, S., and Koizumi, N. (2018). Effect of a p38 Mitogen-Activated Protein Kinase Inhibitor on Corneal Endothelial Cell Proliferation. Invest Ophthalmol Vis Sci *59*, 4218-4227.

Okumura, N., Hirano, H., Numata, R., Nakahara, M., Ueno, M., Hamuro, J., Kinoshita, S., and Koizumi, N. (2014a). Cell surface markers of functional phenotypic corneal endothelial cells. Invest Ophthalmol Vis Sci *55*, 7610-7618.

Okumura, N., Kinoshita, S., and Koizumi, N. (2014b). Cell-based approach for treatment of corneal endothelial dysfunction. Cornea *33 Suppl 11*, S37-41.

Parekh, M., Ferrari, S., Sheridan, C., Kaye, S., and Ahmad, S. (2016). Concise Review: An Update on the Culture of Human Corneal Endothelial Cells for Transplantation. Stem Cells Transl Med *5*, 258-264.

817 Peh, G.S., Chng, Z., Ang, H.P., Cheng, T.Y., Adnan, K., Seah, X.Y., George, B.L., Toh, K.P., Tan, D.T.,
818 Yam, G.H., Colman, A., and Mehta, J.S. (2015). Propagation of human corneal endothelial cells: a novel
819 dual media approach. Cell Transplant *24*, 287-304.

820 Peh, G.S.L., Ang, H.P., Lwin, C.N., Adnan, K., George, B.L., Seah, X.Y., Lin, S.J., Bhogal, M., Liu,
821 Y.C., Tan, D.T., and Mehta, J.S. (2017). Regulatory Compliant Tissue-Engineered Human Corneal
822 Endothelial Grafts Restore Corneal Function of Rabbits with Bullous Keratopathy. Sci Rep *7*, 14149.

823 Peh, G.S.L., Ong, H.S., Adnan, K., Ang, H.P., Lwin, C.N., Seah, X.Y., Lin, S.J., and Mehta, J.S. (2019).
824 Functional Evaluation of Two Corneal Endothelial Cell-Based Therapies: Tissue-Engineered Construct
825 and Cell Injection. Sci Rep *9*, 6087.

826 Pimentel, H., Bray, N.L., Puente, S., Melsted, P., and Pachter, L. (2017). Differential analysis of RNA-
827 seq incorporating quantification uncertainty. Nat Methods *14*, 687-690.

828 Reitsma, S., Slaaf, D.W., Vink, H., van Zandvoort, M.A., and oude Egbrink, M.G. (2007). The
829 endothelial glycocalyx: composition, functions, and visualization. Pflugers Arch *454*, 345-359.

830 Santander-Garcia, D., Ortega, M.C., Benito-Martinez, S., Barroso, S., Jimenez-Alfaro, I., and Millan, J.
831 (2016). A human cellular system for analyzing signaling during corneal endothelial barrier dysfunction.
832 Exp Eye Res *153*, 8-13.

833 Schmedt, T., Chen, Y., Nguyen, T.T., Li, S., Bonanno, J.A., and Jurkunas, U.V. (2012). Telomerase
834 immortalization of human corneal endothelial cells yields functional hexagonal monolayers. PLoS One *7*,
835 e51427.

836 Schroder, H.D., and Sperling, S. (1977). Polysaccharide coating of human corneal endothelium. Acta
837 Ophthalmol (Copenh) *55*, 819-826.

838 Serbecic, N., and Beutelspacher, S.C. (2005). Vitamins inhibit oxidant-induced apoptosis of corneal
839 endothelial cells. Jpn J Ophthalmol *49*, 355-362.

840 Sheerin, A.N., Smith, S.K., Jennert-Burston, K., Brook, A.J., Allen, M.C., Ibrahim, B., Jones, D., Wallis,
841 C., Engelmann, K., Rhys-Williams, W., Faragher, R.G., and Kipling, D. (2012). Characterization of
842 cellular senescence mechanisms in human corneal endothelial cells. Aging Cell *11*, 234-240.

843 Sherrard, E.S. (1976). The corneal endothelium in vivo: its response to mild trauma. Exp Eye Res *22*,
844 347-357.

845 Shima, N., Kimoto, M., Yamaguchi, M., and Yamagami, S. (2011). Increased proliferation and replicative
846 lifespan of isolated human corneal endothelial cells with L-ascorbic acid 2-phosphate. Invest Ophthalmol
847 Vis Sci *52*, 8711-8717.

848 Soh, Y.Q., Peh, G.S.L., and Mehta, J.S. (2017). Translational issues for human corneal endothelial tissue
849 engineering. J Tissue Eng Regen Med *11*, 2425-2442.

850 Spandidos, A., Wang, X., Wang, H., Dragnev, S., Thurber, T., and Seed, B. (2008). A comprehensive
851 collection of experimentally validated primers for Polymerase Chain Reaction quantitation of murine
852 transcript abundance. BMC Genomics *9*, 633.

853 Spandidos, A., Wang, X., Wang, H., and Seed, B. (2010). PrimerBank: a resource of human and mouse
854 PCR primer pairs for gene expression detection and quantification. Nucleic Acids Res *38*, D792-799.

855 Sperling, S., and Jacobsen, S.R. (1980). The surface coat on human corneal endothelium. Acta
856 Ophthalmol (Copenh) *58*, 96-102.

857 Srinivas, S.P. (2010). Dynamic regulation of barrier integrity of the corneal endothelium. Optom Vis Sci
858 *87*, E239-254.

859 Stolwijk, J.A., Matrougui, K., Renken, C.W., and Trebak, M. (2015). Impedance analysis of GPCR-
860 mediated changes in endothelial barrier function: overview and fundamental considerations for stable and
861 reproducible measurements. Pflugers Arch *467*, 2193-2218.

862 Teichmann, J., Valtink, M., Nitschke, M., Gramm, S., Funk, R.H., Engelmann, K., and Werner, C.
863 (2013). Tissue engineering of the corneal endothelium: a review of carrier materials. J Funct Biomater *4*,
864 178-208.

865 Toda, M., Ueno, M., Hiraga, A., Asada, K., Montoya, M., Sotozono, C., Kinoshita, S., and Hamuro, J.
866 (2017). Production of Homogeneous Cultured Human Corneal Endothelial Cells Indispensable for
867 Innovative Cell Therapy. Invest Ophthalmol Vis Sci *58*, 2011-2020.

868 Ueno, M., Asada, K., Toda, M., Nagata, K., Sotozono, C., Kosaka, N., Ochiya, T., Kinoshita, S., and
869 Hamuro, J. (2016). Concomitant Evaluation of a Panel of Exosome Proteins and MiRs for Qualification
870 of Cultured Human Corneal Endothelial Cells. Invest Ophthalmol Vis Sci *57*, 4393-4402.

871 Valtink, M., Gruschwitz, R., Funk, R.H., and Engelmann, K. (2008). Two clonal cell lines of
872 immortalized human corneal endothelial cells show either differentiated or precursor cell characteristics.
873 Cells Tissues Organs *187*, 286-294.

874 Van den Bogerd, B., Dhubhghaill, S.N., Koppen, C., Tassignon, M.J., and Zakaria, N. (2018). A review
875 of the evidence for in vivo corneal endothelial regeneration. Surv Ophthalmol *63*, 149-165.

876 Vithana, E.N., Morgan, P., Sundaresan, P., Ebenezer, N.D., Tan, D.T., Mohamed, M.D., Anand, S.,
877 Khine, K.O., Venkataraman, D., Yong, V.H., Salto-Tellez, M., Venkatraman, A., Guo, K., Hemadevi, B.,
878 Srinivasan, M., Prajna, V., Khine, M., Casey, J.R., Inglehearn, C.F., and Aung, T. (2006). Mutations in
879 sodium-borate cotransporter SLC4A11 cause recessive congenital hereditary endothelial dystrophy
880 (CHED2). Nat Genet *38*, 755-757.

881 Wang, X., and Seed, B. (2003). A PCR primer bank for quantitative gene expression analysis. Nucleic
882 Acids Res *31*, e154.

883 Wieben, E.D., Aleff, R.A., Tosakulwong, N., Butz, M.L., Highsmith, W.E., Edwards, A.O., and Baratz,
884 K.H. (2012). A common trinucleotide repeat expansion within the transcription factor 4 (TCF4, E2-2)
885 gene predicts Fuchs corneal dystrophy. PLoS One *7*, e49083.

886 Yamashita, K., Inagaki, E., Hatou, S., Higa, K., Ogawa, A., Miyashita, H., Tsubota, K., and Shimmura, S.
887 (2018). Corneal Endothelial Regeneration Using Mesenchymal Stem Cells Derived from Human
888 Umbilical Cord. Stem Cells Dev *27*, 1097-1108.

889 Yoshihara, M., Ohmiya, H., Hara, S., Kawasaki, S., consortium, F., Hayashizaki, Y., Itoh, M., Kawaji, H.,
890 Tsujikawa, M., and Nishida, K. (2015). Discovery of molecular markers to discriminate corneal
891 endothelial cells in the human body. PLoS One *10*, e0117581.
892

893 Table 1. Gene ontology and pathway enrichment analysis of the P0 inter-media comparison.

Source	Term Name	Term ID	FDR p-value
F99 Passage 0			
GO:BP	developmental process	GO:0032502	4.2E-18
GO:BP	system development	GO:0048731	1.3E-16
GO:BP	multicellular organism development	GO:0007275	1.1E-15
GO:BP	anatomical structure morphogenesis	GO:0009653	3.6E-15
GO:BP	tissue development	GO:0009888	2.1E-14
GO:BP	cellular developmental process	GO:0048869	7.8E-14
GO:BP	cell differentiation	GO:0030154	2.3E-13
GO:BP	cell development	GO:0048468	3.6E-09
GO:BP	tube development	GO:0035295	3.8E-09
GO:BP	blood vessel development	GO:0001568	4.4E-09
GO:BP	circulatory system development	GO:0072359	4.6E-09
GO:BP	regulation of cell differentiation	GO:0045595	6.0E-09
GO:BP	nervous system development	GO:0007399	1.0E-07
GO:BP	epithelium development	GO:0060429	3.7E-07
KEGG	TGF-beta signaling pathway	KEGG:04350	3.2E-02
WP	miR-509-3p alteration of YAP1/ECM axis	WP:WP3967	5.1E-04
WP	Epithelial to mesenchymal transition in colorectal cancer	WP:WP4239	2.1E-02
WP	Senescence and Autophagy in Cancer	WP:WP615	3.2E-02
M5 Passage 0			
GO:MF	oxidoreductase activity	GO:0016491	1.0E-18
GO:MF	electron transfer activity	GO:0009055	7.9E-16
GO:MF	proton transmembrane transporter activity	GO:0015078	1.3E-12
GO:MF	cytochrome-c oxidase activity	GO:0004129	2.3E-07
GO:MF	NADH dehydrogenase activity	GO:0003954	3.4E-07
GO:BP	oxidative phosphorylation	GO:0006119	4.9E-29
GO:BP	cellular respiration	GO:0045333	5.1E-25
GO:BP	lipid oxidation	GO:0034440	4.0E-05
GO:BP	fatty acid oxidation	GO:0019395	2.1E-04
GO:BP	lipid catabolic process	GO:0016042	9.2E-04
GO:BP	fatty acid metabolic process	GO:0006631	1.1E-03
GO:CC	mitochondrial part	GO:0044429	1.6E-47
GO:CC	mitochondrion	GO:0005739	3.8E-37
KEGG	Oxidative phosphorylation	KEGG:00190	1.5E-31
KEGG	Citrate cycle (TCA cycle)	KEGG:00020	7.0E-05
KEGG	Fatty acid metabolism	KEGG:01212	1.6E-03
WP	Electron Transport Chain (OXPHOS system in mitochondria)	WP:WP111	2.3E-38
WP	Fatty Acid Beta Oxidation	WP:WP143	2.2E-04

894 Note: See Figure S3A for complete set of inter-media comparisons.
895 FDR, false discovery rate; GO, gene ontology; BP, biological process; MF, molecular function; CC,
896 cellular component; KEGG, Kyoto encyclopedia of genes and genomes; WP, WikiPathways.

897 Table 2. Gene ontology and pathway enrichment analysis of the P3 and P4 intra-media comparisons.

Source	Term Name	Term ID	FDR p-value
F99 Passage 3			
GO:BP	system development	GO:0048731	5.1E-06
GO:BP	animal organ development	GO:0048513	1.2E-05
GO:BP	cellular response to stress	GO:0033554	3.4E-04
GO:BP	mitotic cell cycle	GO:0000278	2.9E-03
GO:BP	response to stress	GO:0006950	3.6E-03
GO:BP	regulation of mitotic cell cycle	GO:0007346	1.4E-02
GO:BP	cell differentiation	GO:0030154	2.0E-02
GO:BP	MAPK cascade	GO:0000165	4.0E-02
GO:CC	vesicle	GO:0031982	6.3E-09
GO:CC	endomembrane system	GO:0012505	1.1E-08
KEGG	p53 signaling pathway	KEGG:04115	4.4E-04
KEGG	Focal adhesion	KEGG:04510	1.1E-02
KEGG	Apelin signaling pathway	KEGG:04371	3.3E-02
KEGG	Cellular senescence	KEGG:04218	4.8E-02
REAC	Senescence-Associated Secretory Phenotype (SASP)	REAC:R-HSA-2559582	3.0E-02
REAC	Cell Cycle, Mitotic	REAC:R-HSA-69278	4.2E-02
WP	Wnt Signaling	WP:WP428	1.1E-02
F99 Passage 4			
GO:MF	cyclin-dependent protein serine/threonine kinase inhibitor activity	GO:0004861	3.6E-03
GO:BP	nervous system development	GO:0007399	1.0E-08
GO:BP	response to oxidative stress	GO:0006979	1.2E-07
GO:BP	regulation of programmed cell death	GO:0043067	7.1E-07
GO:BP	apoptotic process	GO:0006915	1.1E-06
GO:BP	cell differentiation	GO:0030154	2.2E-06
GO:BP	mitotic cell cycle	GO:0000278	1.3E-05
GO:BP	aging	GO:0007568	2.4E-02
GO:BP	MAPK cascade	GO:0000165	4.5E-02
GO:CC	vesicle	GO:0031982	1.8E-15
GO:CC	endomembrane system	GO:0012505	3.9E-15
KEGG	Focal adhesion	KEGG:04510	1.0E-06
KEGG	p53 signaling pathway	KEGG:04115	5.8E-05
KEGG	Cellular senescence	KEGG:04218	4.2E-03
KEGG	PI3K-Akt signaling pathway	KEGG:04151	8.5E-03
REAC	Developmental Biology	REAC:R-HSA-1266738	1.5E-02
REAC	Cell Cycle, Mitotic	REAC:R-HSA-69278	3.5E-02
M5 Passage 3			
GO:MF	growth factor binding	GO:0019838	9.6E-04
GO:MF	cyclin-dependent protein serine/threonine kinase regulator activity	GO:0016538	3.2E-03
GO:BP	cell cycle	GO:0007049	1.7E-11

GO:BP	regulation of programmed cell death	GO:0043067	8.0E-07
GO:BP	cell cycle phase transition	GO:0044770	2.4E-06
GO:BP	cell differentiation	GO:0030154	2.0E-05
GO:BP	programmed cell death	GO:0012501	5.2E-05
GO:BP	MAPK cascade	GO:0000165	9.8E-05
GO:BP	response to oxidative stress	GO:0006979	2.1E-04
GO:BP	aging	GO:0007568	1.4E-02
GO:CC	vesicle	GO:0031982	2.2E-18
GO:CC	endomembrane system	GO:0012505	2.8E-08
KEGG	Cell cycle	KEGG:04110	2.9E-06
KEGG	p53 signaling pathway	KEGG:04115	1.1E-03
KEGG	Focal adhesion	KEGG:04510	1.6E-03
KEGG	MAPK signaling pathway	KEGG:04010	3.6E-03
REAC	Cell Cycle, Mitotic	REAC:R-HSA-69278	3.9E-06
M5 Passage 4			
GO:MF	cyclin-dependent protein serine/threonine kinase regulator activity	GO:0016538	3.6E-02
GO:BP	cell division	GO:0051301	2.1E-09
GO:BP	mitotic cell cycle	GO:0000278	1.8E-08
GO:BP	positive regulation of cell death	GO:0010942	4.2E-08
GO:BP	response to oxidative stress	GO:0006979	5.3E-06
GO:BP	cellular response to stress	GO:0033554	7.3E-06
GO:BP	regulation of MAPK cascade	GO:0043408	6.8E-05
GO:BP	electron transport chain	GO:0022900	3.7E-04
GO:BP	exocytosis	GO:0006887	1.4E-03
GO:BP	secretion by cell	GO:0032940	5.8E-03
GO:CC	vesicle	GO:0031982	5.7E-21
KEGG	Focal adhesion	KEGG:04510	2.6E-05
KEGG	MAPK signaling pathway	KEGG:04010	1.0E-03
KEGG	p53 signaling pathway	KEGG:04115	1.5E-03
KEGG	Oxidative phosphorylation	KEGG:00190	3.8E-02
REAC	The citric acid (TCA) cycle and respiratory electron transport	REAC:R-HSA-1428517	2.2E-04
WP	Electron Transport Chain (OXPHOS system in mitochondria)	WP:WP111	6.3E-03

Note: Note: See Figure S3B for complete set of intra-media comparisons.
FDR, false discovery rate; GO, gene ontology; BP, biological process; MF, molecular function; CC, cellular component; KEGG, Kyoto encyclopedia of genes and genomes; REAC, REACTOME; WP, WikiPathways.

903 Table 3: Activation state of Ingenuity canonical pathways in P3 and P4 intra-media comparisons.

Ingenuity Canonical Pathways	**z-score**
F99 Passage 3	
NRF2-mediated Oxidative Stress Response	3.36
IL-8 Signaling	2.89
Apelin Endothelial Signaling Pathway	2.71
Cell Cycle: G2/M DNA Damage Checkpoint Regulation	2.65
Chemokine Signaling	2.33
IL-3 Signaling	2.33
ERK/MAPK Signaling	1.90
VEGF Family Ligand-Receptor Interactions	1.89
IL-6 Signaling	1.89
IGF-1 Signaling	1.67
Acute Phase Response Signaling	1.67
JAK/Stat Signaling	1.41
p53 Signaling	1.13
FGF Signaling	1.00
Estrogen-mediated S-phase Entry	-1.00
Cyclins and Cell Cycle Regulation	-1.13
RhoGDI Signaling	-1.41
LXR/RXR Activation	-2.24
F99 Passage 4	
Cell Cycle: G2/M DNA Damage Checkpoint Regulation	3.46
NRF2-mediated Oxidative Stress Response	3.27
IL-8 Signaling	3.09
Chemokine Signaling	2.89
p53 Signaling	2.83
UVC-Induced MAPK Signaling	2.33
IGF-1 Signaling	1.41
Inflammasome pathway	1.34
Apelin Endothelial Signaling Pathway	1.28
IL-6 Signaling	1.21
IL-1 Signaling	1.13
HGF Signaling	1.00
JAK/Stat Signaling	1.00
Estrogen-mediated S-phase Entry	-1.13
Chondroitin Sulfate Degradation (Metazoa)	-1.34
Pyrimidine Deoxyribonucleotides De Novo Biosynthesis I	-1.34
NER Pathway	-1.90
LXR/RXR Activation	-3.00
M5 Passage 3	
NRF2-mediated Oxidative Stress Response	3.27
Cell Cycle: G2/M DNA Damage Checkpoint Regulation	3.16

Chemokine Signaling	2.71
IL-8 Signaling	2.69
Acute Phase Response Signaling	2.50
IL-6 Signaling	2.32
TGF-β Signaling	2.11
Inflammasome pathway	2.00
IL-1 Signaling	1.89
JAK/Stat Signaling	1.51
p53 Signaling	1.39
p38 MAPK Signaling	1.00
Glycolysis I	-1.00
Fatty Acid β-oxidation I	-1.00
Estrogen Biosynthesis	-1.00
Pyrimidine Deoxyribonucleotides De Novo Biosynthesis I	-2.00
NER Pathway	-2.33
LXR/RXR Activation	-3.00
M5 Passage 4	
NRF2-mediated Oxidative Stress Response	4.60
IL-8 Signaling	3.51
Chemokine Signaling	3.00
IL-6 Signaling	2.84
Cell Cycle: G2/M DNA Damage Checkpoint Regulation	2.67
Inflammasome pathway	2.24
p53 Signaling	2.07
IL-1 Signaling	1.90
Acute Phase Response Signaling	1.88
p38 MAPK Signaling	1.70
JAK/Stat Signaling	1.41
IGF-1 Signaling	1.34
Fatty Acid β-oxidation I	-1.63
Acetyl-CoA Biosynthesis I (Pyruvate Dehydrogenase Complex)	-2.00
Cholesterol Biosynthesis I	-2.00
Superpathway of Cholesterol Biosynthesis	-2.45
TCA Cycle II (Eukaryotic)	-2.65
Oxidative Phosphorylation	-5.11

904 Notes: 1) See Figure S3B for complete set of intra-media comparisons. 2) A positive z-score denotes
905 activation and a negative z-score denotes deactivation.
906

907 Table 4: Activation state of cell cycle functions in P0 and P4 intra-media comparisons.

Function Annotation	**z-score**
F99 Passage 3	
Senescence of cells	0.99
Replicative senescence of cells	0.60
Cell cycle progression	-0.86
Re-entry into interphase	-1.34
Mitosis	-1.72
Initiation of interphase	-1.73
F99 Passage 4	
Senescence of tumor cell lines	1.51
G1 phase	1.35
Senescence of cells	0.69
M phase	-0.53
M phase of cervical cancer cell lines	-0.79
M phase of tumor cell lines	-1.30
M5 Passage 3	
Senescence of cells	1.14
G1 phase	0.90
Cell cycle progression	-0.81
M phase	-1.19
Mitosis	-1.69
Segregation of chromosomes	-2.13
M5 Passage 4	
G1 phase	2.24
Senescence of cells	1.70
Cell cycle progression	-0.88
Cytokinesis	-1.06
M phase	-1.18
Segregation of chromosomes	-1.69

908 Notes: 1) See Figure S3B for complete set of intra-media comparisons. 2) A positive z-score denotes
909 activation and a negative z-score denotes deactivation.

910 **SUPPLEMENTARY TABLES**
911
912 **Table S1.** Donor cornea information

913 **Table S2.** Quantitative PCR primers.

914 **Table S3.** Antibodies.

915 **Table S4.** Differential gene expression lists for inter-media comparisons.

916 **Table S5.** Full results of gene ontology and pathway enrichment in inter-media data sets.

917 **Table S6.** Expression of cell senescence-associated genes in primary CEnC.

918 **Table S7.** Differential gene expression lists for intra-media comparisons.

919 **Table S8.** Full results of gene ontology and pathway enrichment in intra-media data sets.

920 **Table S9.** Full results of activation of Ingenuity canonical pathway in intra-media data sets.

921 **Table S10.** Full results of activation of Ingenuity cell cycle functions in intra-media data sets.